

KfK 5407
November 1994

MHD-Channel Flow Related to Self-cooled Liquid-metal Blanket Development

L. Bühler, U. Müller
Institut für Angewandte Thermo- und Fluidodynamik
Projekt Kernfusion

Kernforschungszentrum Karlsruhe

Kernforschungszentrum Karlsruhe
Institut für Angewandte Thermo- und Fluidodynamik
Projekt Kernfusion

KfK 5407

MHD – Channel flow related to
self – cooled liquid – metal blanket development

L. Bühler, U. Müller

Kernforschungszentrum Karlsruhe GmbH, Karlsruhe

Als Manuskript gedruckt
Für diesen Bericht behalten wir uns alle Rechte vor

Kernforschungszentrum Karlsruhe GmbH
Postfach 3640, 76021 Karlsruhe

ISSN 0303-4003

MHD – Channel flow related to self – cooled liquid – metal blanket development

Abstract

The reliable design of fusion blankets using liquid-metals as coolant or breeding material requires detailed knowledge and computational tools for predicting pressure losses and flow pattern associated with the flow of the electrically conducting fluid in the region of the strong plasma-confining magnetic field. Magnetohydrodynamic flows have been investigated in the past by a number of researchers all over the world. Especially the problems arising from the MHD flows in complex three-dimensional elements of fusion blankets have been analyzed so that there exists a quite good understanding of the flow behaviour in the basic geometric elements like straight ducts, expansions, contractions, bends with different orientations with respect to the magnetic field, manifolds, and electrically coupled parallel ducts or bends. This report will address all these flow types, to give the main references for more detailed information, and to summarize the scientific contribution and progress achieved at the *Institut für Angewandte Thermo- und Fluidodynamik* of the *Kernforschungszentrum Karlsruhe*.

MHD Kanalströmungen für die Entwicklung von selbstgekühlten Fusions – Blankets

Zusammenfassung

Zuverlässige Entwürfe von Fusions–Blanket Konzepten, bei denen Flüssig–Metalle als Kühlmittel oder als Brutstoff eingesetzt werden, erfordern die genaue Kenntnis der Druckverluste und der Geschwindigkeitsverteilung von Strömungen elektrisch leitender Fluide im Bereich der starken Magnetfelder, die das Fusionsplasma einschließen, und es müssen Berechnungsprogramme vorhanden sein, um diese zu bestimmen. In der Vergangenheit wurden magnetohydrodynamische Strömungen weltweit von vielen Wissenschaftlern untersucht. Speziell untersucht wurden Strömungsprobleme in komplizierten dreidimensionalen Elementen von Fusions–Blankets, so daß heute das Strömungsverhalten in den wichtigsten Geometrien gut verstanden ist. Solche Geometrien sind z.B. gerade Kanäle, Erweiterungen, Verengungen, Krümmer mit unterschiedlicher Orientierung bezüglich des magnetischen Feldes, Verzweigungen sowie elektrisch gekoppelte Kanäle und Krümmer. Dieser Bericht spricht alle diese Strömungstypen an mit dem Ziel, Literaturhinweise für detailliertere Informationen zu geben und die wissenschaftlichen Beiträge und Fortschritte zusammenzufassen, die am *Institut für Angewandte Thermo– und Fluidodynamik des Kernforschungszentrums Karlsruhe* auf diesem Gebiet erarbeitet wurden.

This report should be not considered as the work obtained by the authors, but as a summary of main results obtained during the last years at the *Institut für Angewandte Thermo- und Fluidodynamik* of the *Kernforschungszentrum Karlsruhe*. Contributions to the results have been made by

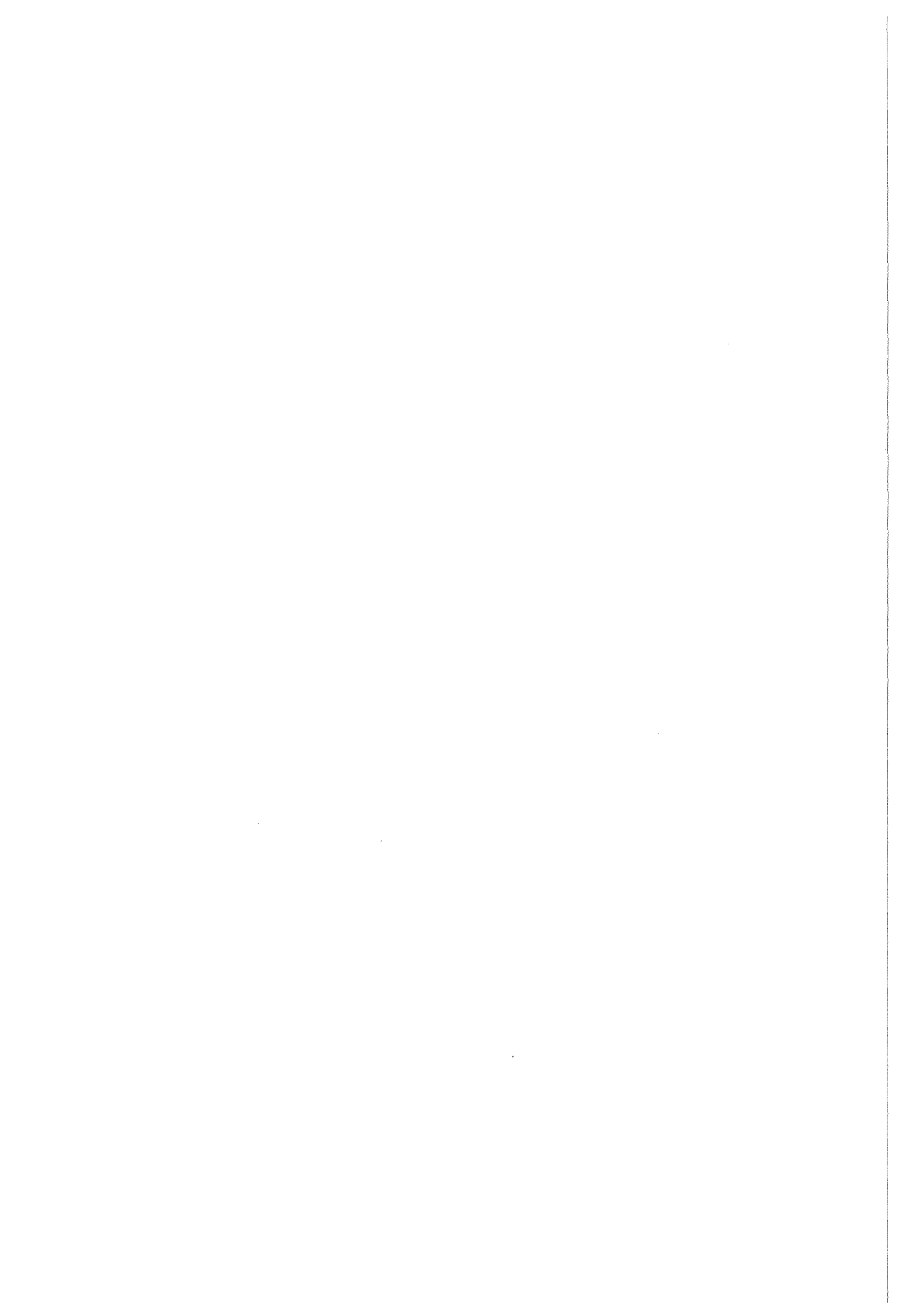
Barleon, L.,
Bühler, L.,
Leboucher, L.,
Lenhart, L.,
Malang, S.,
McCarthy, K.A.,
Molokov, S.,
Müller, U.,
Reimann, J.,
Sterl, A.,
Stieglitz, R.,
Burr, U.

with the technical support of

Kreuzinger, H.,
Mack, K.J.,
Thomauske, K.,
Vollmer, R.

in collaboration with

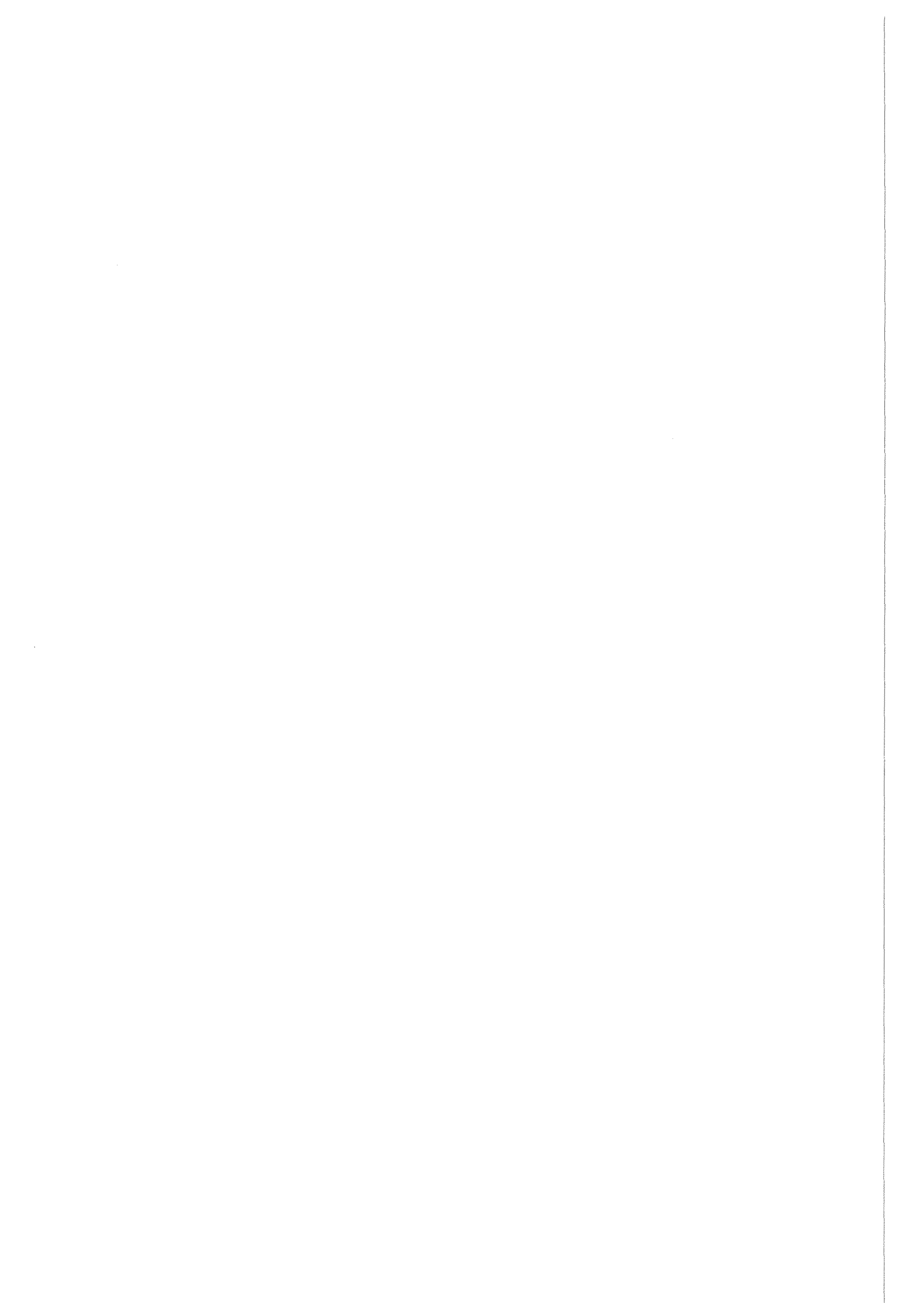
Argonne National Laboratory (Argonne, Il., USA),
Latvian Academy of Science (Riga, Latvia).



MHD-Channel flow related to self-cooled liquid-metal blanket development

Contents

1 Introduction	9
2 Basic physics	12
2.1 Governing equations and boundary conditions	12
2.2 MHD Phenomena	14
3 Methods for solution	16
3.1 Direct numerical solution	16
3.2 Asymptotic solutions	17
4 Experimental methods	19
4.1 The experimental setup	19
4.2 Measuring techniques	21
4.2.1 Integral quantities	21
4.2.2 Local quantities	21
4.3 Data acquisition system	24
5 Flows in hydraulic elements	25
5.1 Straight duct flow	25
5.1.1 Fully developed flows	25
5.1.2 Methods for pressure drop reduction	28
5.1.3 3D effects in straight duct flows	32
5.2 Variable cross section area	35
5.2.1 Expansions, contractions	35
5.2.2 Flow in a complex geometry of a blanket element	38
5.3 Bends	40
5.3.1 Bends in the plane perpendicular to the magnetic field	41
5.3.2 Bends in the plane of the magnetic field	41
5.4 Multi-channel flows	53
5.4.1 Straight duct flows	54
5.4.2 Multi-bend flows	56
6 Conclusions	69



1 Introduction

Fusion blankets are essential components of fusion power reactors in which the high neutron and γ -radiation energy from the plasma is transferred to utilisable thermal energy and where, moreover, the fuel component tritium is bred by neutron reaction. Self-cooled liquid metal blankets are particularly attractive because of the excellent cooling capability of liquid metal and because they can be designed as a simple and robust self-supporting structure of coolant channels.

As the blankets have to be placed within the plasma-confining strong magnetic fields (4–7 Tesla) of a Tokamak reactor, the electrically well conducting coolant encounters strong electromagnetic forces which may give rise to pressure losses intolerable with regard to the structural stresses and may generate local flow distributions in the channels unfavourable for uniform cooling of the plasma facing first wall. Therefore a detailed knowledge of the MHD-characteristics of liquid metal flow in coolant channels and systems is of crucial importance for the proper design of self-cooled blankets. Several designs have been proposed in the past and rejected because the MHD design feasibility could not be demonstrated clearly (Strandbridge *et al.*, Mitchel & George 1972, Badger *et al.* 1974). More recently in a *Blanket Comparison and Selection Study* of the Argonne National Laboratory (Smith *et al.* 1984) a so-called poloidal-toroidal self-cooled blanket concept has been considered, which showed quite favourable features compared to designs based on other coolants. This has been further advanced at the Nuclear Research Center Karlsruhe for the development of a *European Fusion DEMO* reactor (Malang *et al.* 1988).

A principle sketch of this blanket is shown in figure 1. There are 48 outboard blanket segments in the DEMO-reactor into which the liquid metal coolant enters at the top end, runs down in four large diameter poloidal ducts at the rear side, turns around 180° at the lower end and flows up in poloidal, slightly slanted channels at the central part. The coolant is diverted into small diameter ducts and further on into toroidal ducts arranged in a meander pattern to ensure sufficient cooling of the first wall. From the toroidal parallel channel system the coolant is collected in central slanted poloidal channels again and leaves the blanket at the top end. The inboard blankets differ from the outboard ones by being composed of two parts of similar kind to be installed and/or removed from the upper or lower side of the plasma chamber respectively (see figure 1a).

The poloidal-(radial)-toroidal flow concept has the following characteristic features: In the toroidal channels along the first wall high velocities can be tolerated at, mainly hydraulic pressure losses since the main flow direction coincides with the direction of the

magnetic field. Due to the mean flow there are no induction effects so that high velocities assuring good convective heat transfer at the first wall may be obtained at moderate pressure drop. In the poloidal ducts the flow is mainly perpendicular to the magnetic field so that the electromagnetic forces may cause high pressure losses proportional to the fluid velocities. Therefore the velocities are reduced by choosing large diameter poloidal coolant channels. These pressure drops depend directly on the induced currents which are limited by the electric resistance of the current circuit (including the walls). Therefore, channel walls have either to be relatively thin with regard to the channel diameter or to be at least partly electrically insulating as the pressure losses are in good approximation linearly dependent on the wall thickness and its electrical conductivity.

To achieve acceptable MHD pressure losses the conducting walls should be made as thin as possible (0.5mm or even thinner). Since it is impossible to build up a stiff blanket structure by such walls one introduces an electric decoupling of the load carrying walls from the liquid metal. One possibility to achieve this is to employ *Flow Channel Inserts* (FCI) (Malang *et al.* 1986). These means consist of a thin electrically insulating ceramic layer sandwiched between two thin steel sheets which are welded together at all edges. These layered sheets are shaped to be fitted loosely to the duct inside walls such that the pressure equalization between the flow domain and the duct wall is warranted.

Another method to insulate the channel walls electrically is to cover the channel walls directly by insulating coatings such as aluminum oxide or other ceramic materials. This method is considered the more advanced engineering approach, however, the technological feasibility of the coating process has not yet been demonstrated while some progress with the FCI-technique has been achieved (John, Malang, Sebening (editors) 1991). Therefore this technique is presently considered the reference solution for an electric insulation of the liquid metal cooled blankets discussed in this report.

Another MHD effect in liquid metal cooled blankets is the electric current interaction between different cooling channels of parallel arrangements. This effect may drastically increase the pressure drop in the cooling channels and lead to non uniform volumetric fluxes in different channels. An adequate electric decoupling of parallel channels is a design requirement for self-cooled liquid metal blankets.

A purely poloidal blanket concept is a challenging task regarding simplicity of construction and higher component reliability due to reduced welding joints and certainly is the ultimate design goal for self-cooled blankets. Such a concept has been repeatedly discussed under several slightly different modifications. In principle it contains the same features as the poloidal-toroidal blanket design depicted in figure 1 except that the radial-toroidal channels are missing so that the coolant flows in purely

poloidal channels upward at the plasma-facing side. It has been shown that such a blanket design would lead to coolant pressures beyond or at most too close to the structural limits, if the heat transfer is based on laminar MHD flows. Only if a considerable heat transfer enhancement by turbulence promotion in the coolant flow by at least a factor of two or more compared to laminar flow conditions can be taken into account, a poloidal design will become thermohydraulically feasible. This underlines the research needs to further develop turbulence theory for MHD flows.

Both designs contain several typical hydraulic components whose MHD performance has to be analyzed theoretically or by experimental investigations in order to predict accurately pressure losses and flow distribution. Considering figure 1 one easily identifies pipe or channel expansions and contractions, pipe bends under different orientations to the magnetic field lines, arrangements of parallel channels or bends with conducting walls, and manifolds for splitting or combining the flow.

The theoretical analysis and the experimental investigation of the MHD flow in such hydraulic component is presented in this report.

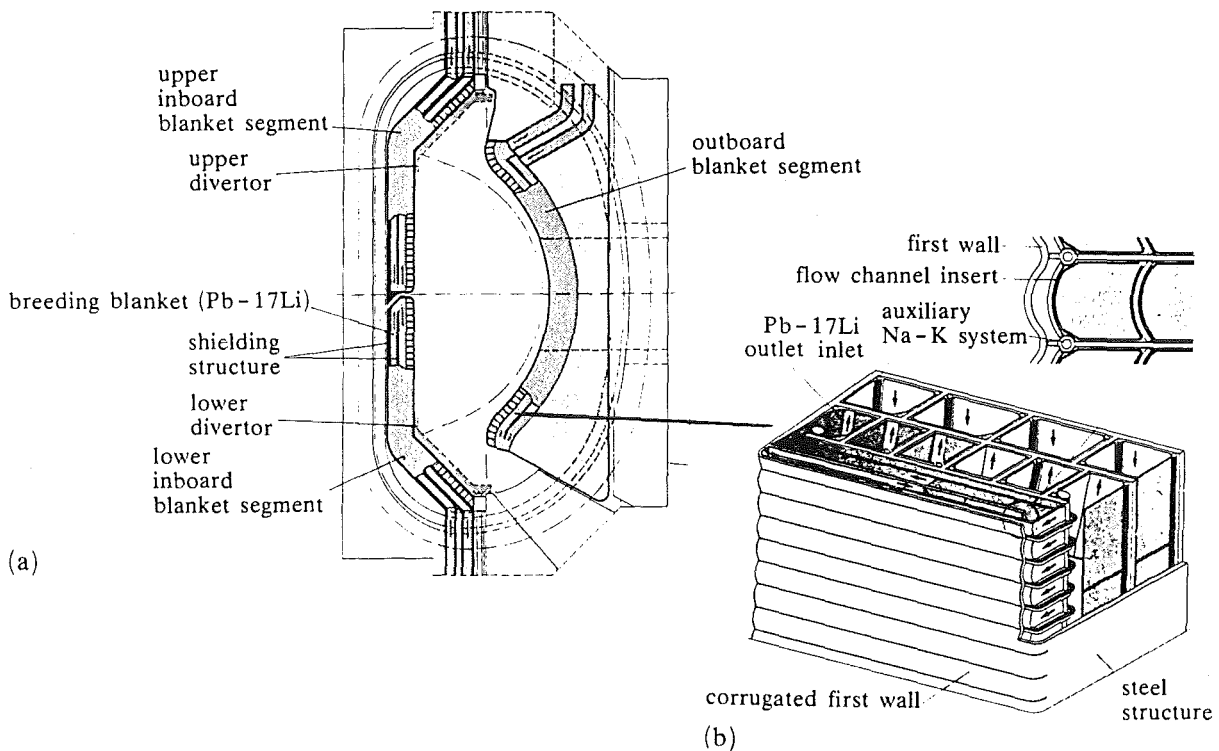


Figure 1 a) Arrangement of self-cooled blankets in a DEMO reactor.
b) Cross section of an outboard segment (Malang *et al.* 1993).

2 Basic physics

2.1 Governing equations and boundary conditions

The flow of an electrically conducting fluid within the applied strong magnetic field confining the fusion plasma may be described by the following non-dimensional equations accounting for the conservation of

$$\text{momentum} \quad \frac{1}{N} \left[\frac{\partial \mathbf{v}}{\partial t} + (\mathbf{v} \cdot \nabla) \mathbf{v} \right] = -\nabla p + \frac{1}{M^2} \nabla^2 \mathbf{v} + \mathbf{j} \times \mathbf{B}, \quad (2.1)$$

$$\text{mass} \quad \nabla \cdot \mathbf{v} = 0, \quad (2.2)$$

$$\text{charge} \quad \nabla \cdot \mathbf{j} = 0, \quad (2.3)$$

and by

$$\text{Ohm's law} \quad \mathbf{j} = -\nabla \phi + \mathbf{v} \times \mathbf{B}. \quad (2.4)$$

The non-dimensional variables $\mathbf{v}, \mathbf{B}, \mathbf{j}, p$, and ϕ , denote velocity, magnetic induction, current density, pressure, and electric potential, scaled by the reference values $v_0, B_0, \sigma v_0 B_0, \sigma L v_0 B_0^2$, and $L v_0 B_0$. The fluid properties like the density ρ , the viscosity ν , and the electric conductivity σ are assumed to be constant. v_0 is the average velocity in a cross section where L is a characteristic length; B_0 is the magnitude of the applied magnetic field induction.

The relative importance of electromagnetic effects compared to inertia effects is given by the

$$\text{interaction parameter} \quad N = \frac{\sigma L B_0^2}{\rho v_0}, \quad (2.5)$$

compared to viscous effects by the square of the

$$\text{Hartmann number} \quad M = L B_0 \sqrt{\frac{\sigma}{\rho \nu}}. \quad (2.6)$$

The ratio of the induced magnetic field to the applied strong field is determined by the

$$\text{magnetic Reynolds number} \quad Re_m = \mu \sigma v_0 L \quad (2.7)$$

and the conductance properties of the wall. For Fusion applications the induced fields are small compared to the applied strong field (see e.g. Hua & Picologlou 1990, Moon et al. 1990). Thus, the applied field remains unchanged by the fluid motion. This fact justifies the inductionsless approximation of equations (2.1-2.4).

The boundary conditions for the flow variables at channel walls are the

$$\text{no-slip condition} \quad \mathbf{v} = 0 \quad (2.8)$$

and the

$$\text{thin-wall condition} \quad \mathbf{j} \cdot \mathbf{n} = \nabla_w \cdot (c \nabla_w \phi_w) , \quad (2.9)$$

which describes the continuity of currents across the fluid wall interface. The current leaving the fluid region inverse to the direction of the inward wall-normal \mathbf{n} enters the wall and creates there a potential ϕ_w . Here ∇_w stands for the components of the gradient vector in the plane of the wall. The

$$\text{wall conductance ratio} \quad c = \frac{\sigma_w t}{\sigma L} \quad (2.10)$$

characterizes the relative conductance of the wall with the conductivity σ_w and thickness t compared to the conductance of the fluid domain.

The potential of the wall is related to the fluid potential by

$$\mathbf{j} \cdot \mathbf{n} = \frac{1}{\kappa} (\phi_w - \phi) , \quad (2.11)$$

where κ is the contact resistance or the resistance $\rho_i \delta_i$ of a thin insulating coating (resistivity ρ_i , thickness δ_i) scaled by L/σ . For a perfect contact between the fluid and the wall, $\kappa=0$, the fluid potential at the wall is equal to the wall potential, $\phi=\phi_w$, whereas for a perfect insulation, as $\kappa \rightarrow \infty$, the wall normal component of current vanishes.

At the entrance and exit of the fluid domain considered the flow is assumed to be either fully developed or given.

2.2 MHD Phenomena

The main physical effects described by equations (2.1-2.11) are explained by the following simple considerations. First, the example of fully developed two-dimensional (2D) MHD flow in straight ducts is considered. Three-dimensional (3D) effects are discussed by heuristic arguments.

At the fusion relevant values of high Hartmann numbers $M \gg 1$ the flow exhibits an inviscid core surrounded by viscous boundary layers at the walls (see fig. 2.1). In the core the interaction $\mathbf{v} \times \mathbf{B}$ of the moving fluid with the magnetic field drives the current of density \mathbf{j} perpendicular to the field and perpendicular to the fluid motion. The interaction of this current with the field causes the *Lorentz force* $\mathbf{j} \times \mathbf{B}$ opposing the fluid motion and thus creating the main part of the high MHD pressure drop. The induced currents complete their circuit in the layers where $\mathbf{v} \times \mathbf{B}$ is reduced due to viscous effects. Since these layers are very thin (*Hartmann layers* of thickness $\delta_H = O(M^{-1})$ at walls perpendicular to \mathbf{B} , or *side layers* with $\delta_S = O(M^{-\frac{1}{2}})$ at walls aligned with \mathbf{B}) it is obvious that they provide the main electric resistance in the current path and determine the pressure drop in insulating ducts ($\kappa = \infty$).

$$\nabla p = O(M^{-1}). \quad (2.12)$$

If the walls are in perfect contact with the fluid ($\kappa = 0$) and better conducting than the viscous layers ($c \gg M^{-\frac{1}{2}}$) the main electric resistance is not longer determined by the layers since almost all the returning current now is flowing inside the wall. The total current is much larger than for the insulating case and results in a pressure gradient

$$\nabla p = O(c),$$

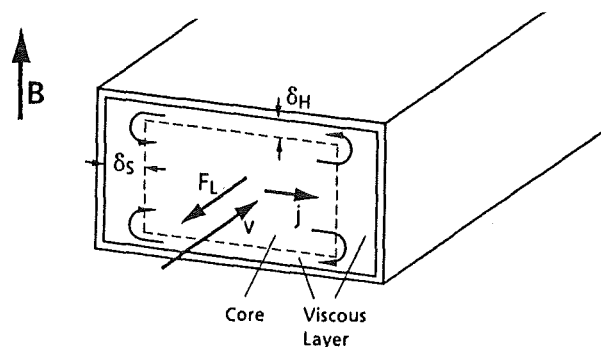


Figure 2.1 Sketch of geometry

if c is still small. In ducts with highly conducting walls, as $c \rightarrow \infty$, the resistance against currents is provided only by the core. This leads to highest currents and to a pressure gradient

$$\nabla p = O(1). \quad (2.13)$$

3D effects in MHD flows occur if the induced potential difference between the sides varies in axial direction. Such variations are possible because of a non-uniform magnetic field at the ends of the magnet, a reduced x -component of velocity observed in expansions or bends, or because of varying conductance properties of the channel walls (see figure 2.2). All these effects cause an axial potential gradient which drives additional currents \mathbf{j}_{3D} inside the fluid. In one part of the duct the current density \mathbf{j}_{3D} has the same direction as the 2D currents of the fully developed flow and gives additional contributions to the pressure gradient. Further down stream \mathbf{j}_{3D} is in opposite direction as the 2D currents. Here it creates a Lorentz force acting in the flow direction. This leads to some pressure recovery. In the first part of the duct mechanical energy is transferred into electrical energy (generator effect). Since the transmission to the second part suffers from Ohm's dissipation only a part can be recovered downstream as mechanical energy (pump effect). Therefore, a pressure drop Δp_{3D} remains irreversibly lost. The axial components of \mathbf{j}_{3D} cause Lorentz forces which displace the fluid towards the sides. Finally a flow pattern is established in the 3D region with a significantly reduced velocity in the center and an increased velocity near the side walls. These simple considerations demonstrate that 3D effects can not be excluded by the use of poorly conducting or insulating channel walls because the currents \mathbf{j}_{3D} take their path inside the fluid itself.

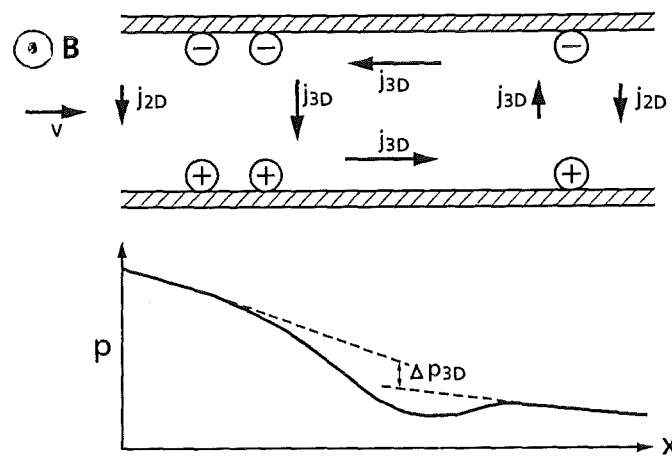


Figure 2.2 Sketch of currents and pressure in 3D flows

3 Methods for solution

Analytical solutions to the problem (2.1-2.11) are restricted to very special cases of boundary conditions and only to simple duct geometries in fully developed flows (Hartmann 1937, Shercliff 1956, Hunt 1965, Gold 1967). Two methods have been used to determine the unknown flow variables in cases of more general applications. One is the completely numerical approach accounting for all physical effects, but restricted in its applicability to MHD flows in basic rectangular duct geometries at moderate values of $M \leq 100$. The other approach focuses to the main physical contributions using asymptotic methods.

3.1 Direct numerical simulation

Attempts for direct numerical simulation (DNS) of MHD flows on the basis of equations (2.1-2.11) have been made by several authors. The preferred numerical methods are finite difference or finite volume methods (Aitov *et al.* 1979, Kim *et al.* 1989, etc.). In the following the method used by Sterl (1990) and later by Lenhart (1994) is addressed in some detail. These authors take advantage of the use of fast Poisson solvers for the evaluation of pressure and potential. Starting from a guessed initial flow field they reach the steady state solution in which they are only interested in by solving the basic equations in the time dependent form. They are more interested in fast convergence than in a precise modeling of the time dependence.

The iteration procedure starts with a Poisson equation for potential, which results from a combination of equation (2.3) and (2.4),

$$\Delta \phi = \nabla \cdot (\mathbf{v} \times \mathbf{B}), \quad (3.1)$$

ensuring conservation of charge. Once the potential is known the currents can be determined using Ohm's law.

In the proceeding step the artificial "velocity" defined as $\mathbf{v}^* = \mathbf{v} + \nabla p$ is calculated by the use of equation (2.1). The pressure p is calculated from the Poisson equation

$$\Delta p = \nabla \cdot \mathbf{v}^*, \quad (3.2)$$

which ensures a solenoidal velocity

$$\mathbf{v} = \mathbf{v}^* - \nabla p . \quad (3.3)$$

This procedure is repeated until the desired steady state solution is reached with sufficient accuracy. While the case of perfectly insulating or conducting walls can be treated directly by applying the relevant standard boundary condition ($\partial\phi/\partial\mathbf{n}=0$ or $\phi=const$) to the Poisson equation (3.3) (Lenhart 1994) the arbitrary wall conductivity requires in addition the solution of equation (2.9) during each iteration step (Sterl 1990). Lenhart introduces domain decomposition techniques for a modeling of more complex geometries by a coupling of basic rectangular subdomains and higher order upwind schemes as an approximation for inertial terms.

For accurate results obtained by DNS the used numerical grid spacing has to be so small that even the thin Hartmann layers are resolved. This fact leads especially for 3D application to an enormous amount of required storage and execution time even on modern vector computers, which finally limits the applicability of DNS to Hartmann numbers $M \leq 100$, significantly smaller than fusion relevant values of $M=10^4-10^5$. Nevertheless, one should consider DNS as an appropriate solution method for fundamental research of elementary MHD problems at moderate Hartmann numbers.

3.2 Asymptotic solution

Asymptotic methods (AM) have often been used to calculate MHD flows in the range of fusion relevant Hartmann numbers (e.g. McCarthy 1989, Madarame & Hagiwara 1989, Hua & Walker 1989 etc.) since they have been proposed for 3D applications by Kulikovskii (1968). The idea is to get a tractable mathematical problem by simplifying the basic equations in such a form that the main physical behavior remains unchanged.

In many fusion applications the interaction parameter N is high enough that inertial terms can be neglected completely. This leads to a linear system of equations. In a next step the flow is divided into one (ore more) core region(s) in which the viscous effects are unimportant at large Hartmann numbers. The cores are separated from each other or from the walls by thin viscous layers. These assumptions lead to considerable simplifications of the equations governing the flow in the cores (subscript c).

$$\nabla p = \mathbf{j}_c \times \mathbf{B} , \quad \nabla \cdot \mathbf{v}_c = 0 , \quad (3.4, 3.5)$$

$$\mathbf{j}_c = -\nabla\phi + \mathbf{v}_c \times \mathbf{B} , \quad \nabla \cdot \mathbf{j}_c = 0 . \quad (3.6, 3.7)$$

From equation (3.4) it follows directly that the pressure and the current components perpendicular to \mathbf{B} do not vary in the direction of \mathbf{B} . This fact allows an easy analytical integration of all equations along the field lines. As integration constants the potential values at the walls are introduced. After the integration the whole 3D problem is reduced to a set of coupled 2D equations governing the pressure in the plane perpendicular to \mathbf{B} and the potential (equation (2.9)) at the fluid wall interface.

More detailed consideration which account in addition to the previous equations (3.4-3.7) for viscous effects lead to the result that the pressure and the potential are constant to the main order of approximation across layers in which the normal component of the magnetic field does not vanish. The decay of the velocity and the variation of current towards the wall is exponential.

$$\mathbf{v} = \mathbf{v}_C(1 - e^{-\eta}) , \quad (3.8)$$

$$\mathbf{j} = \mathbf{j}_C - (\mathbf{j}_C + \nabla_w \phi) e^{-\eta} . \quad (3.9)$$

Here η represents the boundary layer coordinate along the inward wall-normal direction \mathbf{n} , stretched with $M(\mathbf{B} \cdot \mathbf{n})$. At the wall where $\eta=0$ the velocity satisfies the no-slip condition and the tangential currents are given by Ohm's law for a media at rest. Far from the walls as $\eta \rightarrow \infty$ all variables reach the core values. At walls exactly aligned with the magnetic field the modelling is different. For details see (Walker 1981, Bühler 1994).

For the solution of the set of coupled 2D equations two approaches are used. One is iterative with underrelaxation for small values of c (Molokov & Bühler 1994). The use of fast Poisson solvers restricts its applicability to ducts, whose surface is composed by rectangular geometries. The solution procedure is relatively fast and allows a high numerical resolution and even the modeling of 3D MHD flows in a number of coupled subchannels.

The other approach (Bühler 1993,1994) uses boundary-fitted coordinates mapping the arbitrary duct geometry to a standard volume for which the integration and the 2D numerical solution is obtained. The arbitrary coordinate transformation allows non-equidistant grid spacing with high resolution of 3D-regions. The resulting algebraic system is solved by a direct linear solver.

4 Experimental methods

In order to investigate the key features of liquid metal flows in strong magnetic fields two main components are needed, a liquid metal loop and magnets of sufficiently strength supplying a rather homogeneous magnetic field. In the following we give an overview and a short description of the liquid metal loop, the magnets and the measuring techniques used in the MEKKA-facility of the Kernforschungszentrum Karlsruhe. A more detailed description has been given previously by Barleon *et al.* 1989, or Barleon, Casal & Lenhart 1991.

4.1 The experimental setup

Two magnets are available in the MEKKA-facility. There is a normal conducting dipole magnet providing a transverse magnetic field. Its maximum field strength is 2.1 Tesla. The test volume of constant magnetic field strength amounts to 0.17m x 0.48m x 0.8m. The other magnet is the super-conducting solenoid magnet CELLO with a maximum field strength of 3.6 Tesla. The test volume of constant field strength is 0.4m in diameter and 0.45m in length.

An eutetic sodium-potassium alloy ($\text{Na}^{24}\text{K}^{78}$) with a lower density and a higher electrical conductivity compared to a lead-lithium alloy Pb-17Li foreseen in the blanket design is used in the liquid metal loop in order to scale from experimental conditions to fusion blanket relevant conditions. The thermophysical transport properties of the sodium-potassium alloy is given by O'Donnel, Papanikolaou & Reed 1989.

In figure 4.1 a sketch of the liquid metal loop is shown. A canned motor pump with a maximum pressure head of 0.9MPa at a flow rate of 25m³/h circulates the liquid metal at temperatures below 250°C. An additional electromagnetic pump is used for very low flow rates and for high temperature runs. The entire loop can be moved on rails together with the connected test sections along the axis of each magnet. This allows a good access to the instrumented locations of the test sections and variable positioning of the test section within the magnets.

Due the technical features of the loop and the magnets the MEKKA facility is capable of attaining Interaction parameters in the range of $N=10^2-10^5$ at Hartmann numbers up to $M=10^4$, which are present in liquid-metal cooled fusion blankets.

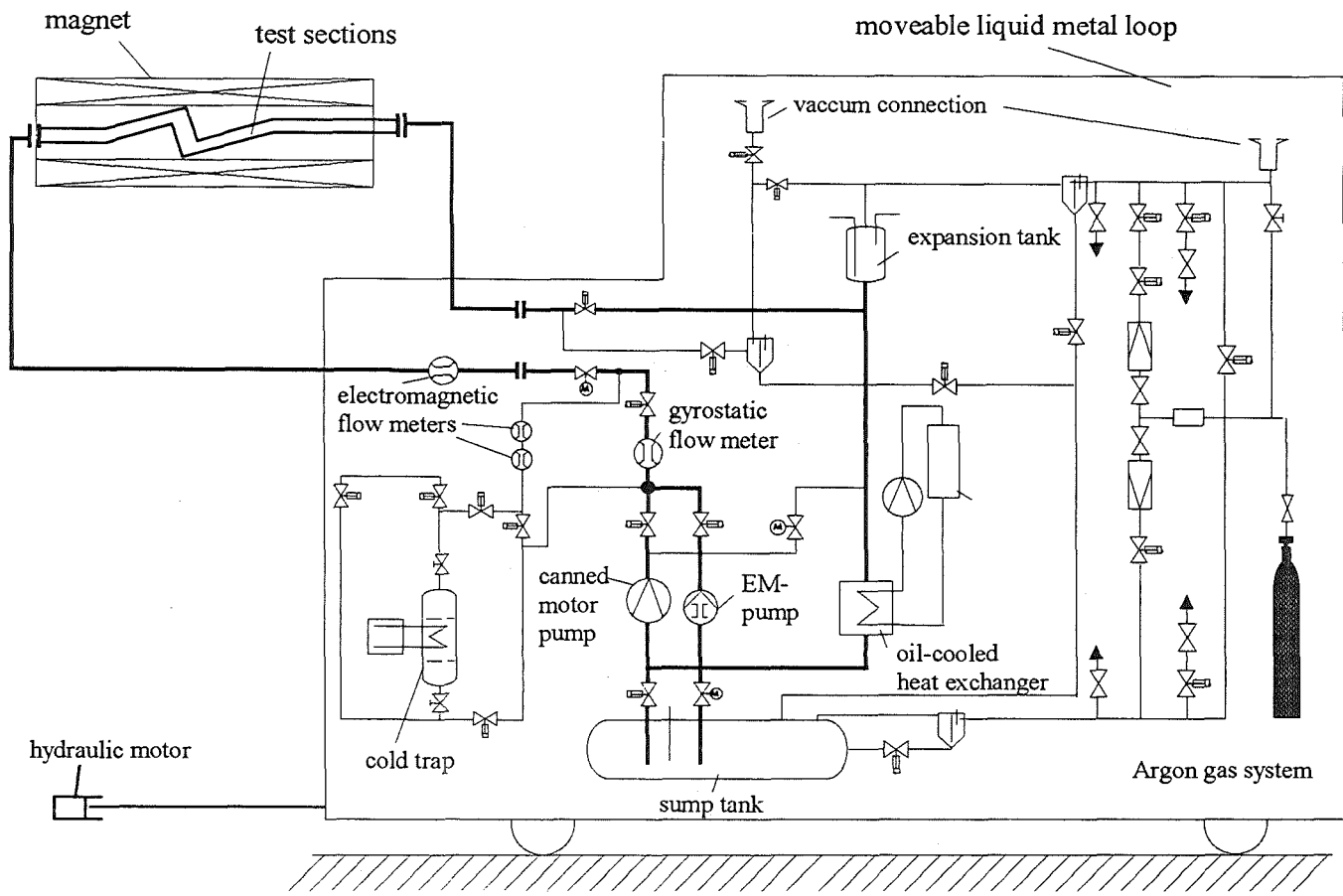


Figure 4.1 The experimental facility

4.2 Measuring techniques

4.2.1 Integral quantities

The flow rate in the loop is measured by two flow meters, which are integrated in the liquid metal loop and use different measuring principles. The gyrostatic flow meter is measuring temperature-independent the total mass flow. Its measuring range is electronically free selectable from 0–3.84tons/h up to 25tons/h. The maximum measuring error in the selected range is 0.3% of the chosen upper limit.

Additionally electromagnetic (EM-) flow meters are used. Due to the small extensions they can be used rather flexible without any changes in the piping system. They are for example used in multi-channel experiments. To avoid any disturbances of the measuring magnetic field of the flow meters by the scattering field of the 'big' magnets they are shielded with ferro-magnetic plates. The accuracy of the EM-flow meters is only restricted to the resolution of the data acquisition system.

The temperatures determining the physical properties of the fluid are measured in case of isothermal experiments at the inlet and outlet of the loop with Ni–NiCr thermocouples.

4.2.2. Local quantities

The MHD-flow at high Hartmann numbers and interaction parameters is determined once the pressure in the duct and the distribution of the electrical potential on the duct surface are known.

To measure the pressure differences in the test sections two different systems of pipes are used in which five or three unipolar capacitive pressure transducers of different measuring range are arranged in series (see figure 4.2). To avoid errors in the pressure difference measurement due to non-linearities of the pressure transducers at their upper limitation the measuring ranges were chosen as to overlap.

For the pressure difference measurements in MHD-flows some effects completely unknown to ordinary hydrodynamics have to be taken into account.

Electrical currents induced in the duct can short circuit in electrically conducting measuring pipes and as a consequence they may have a feedback through the flow in the duct. Therefore the measuring pipes should be made of insulating materials such as rubber.

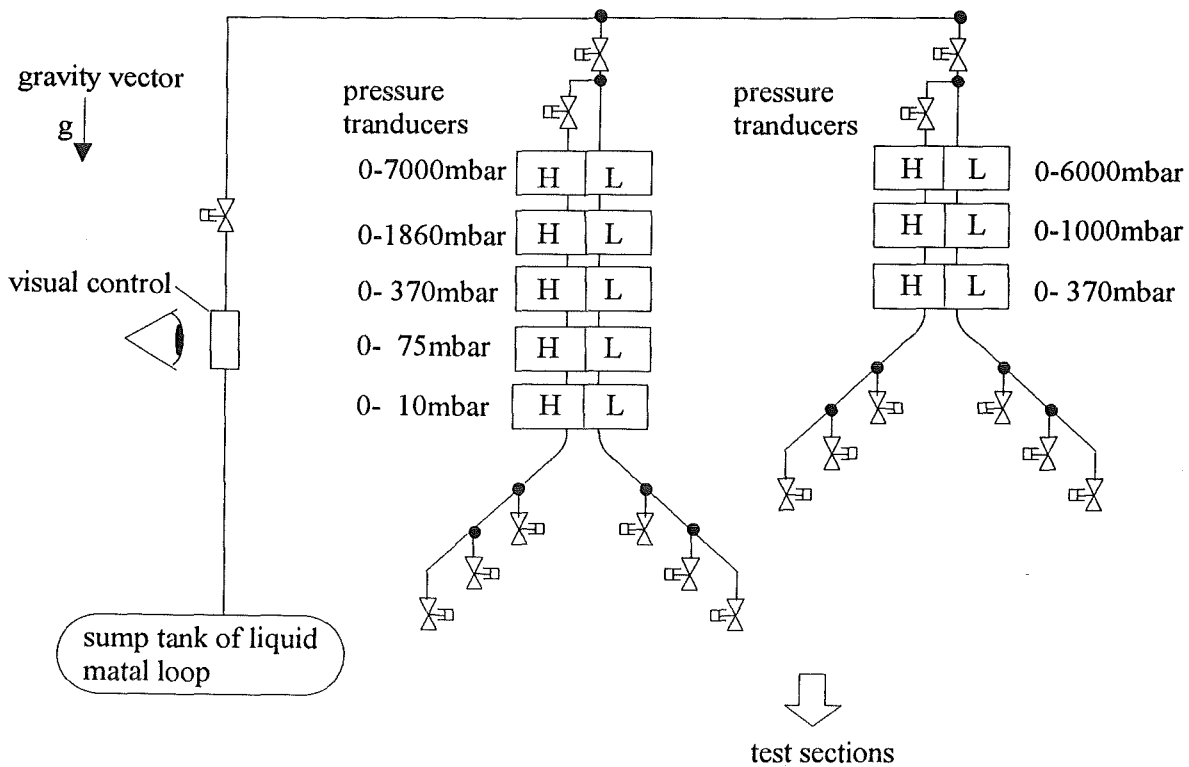


Figure 4.2 Arrangement of pressure transducers

In three-dimensional MHD-flows even another phenomenon is observed. The directly measured pressure represents not the real pressure at the fluid-wall interface. A virtual pressure difference δp is superimposed to the real pressure at each position, caused by electrical currents flowing in the pressure taps perpendicular to the applied magnetic field (in particular if there is a component of the magnetic field tangential to the wall). This virtual pressure difference can be corrected by measuring the electrical potential at each tap, see figure 4.3. The pressure correction δp at the tap can be calculated using the relation

$$\delta p = -\frac{t}{d}(\phi_1 - \phi_2), \quad (4.1)$$

where t is the wall thickness of the duct, d the diameter of the pressure tap and ϕ_1 and ϕ_2 the dimensionless potentials across the tap.

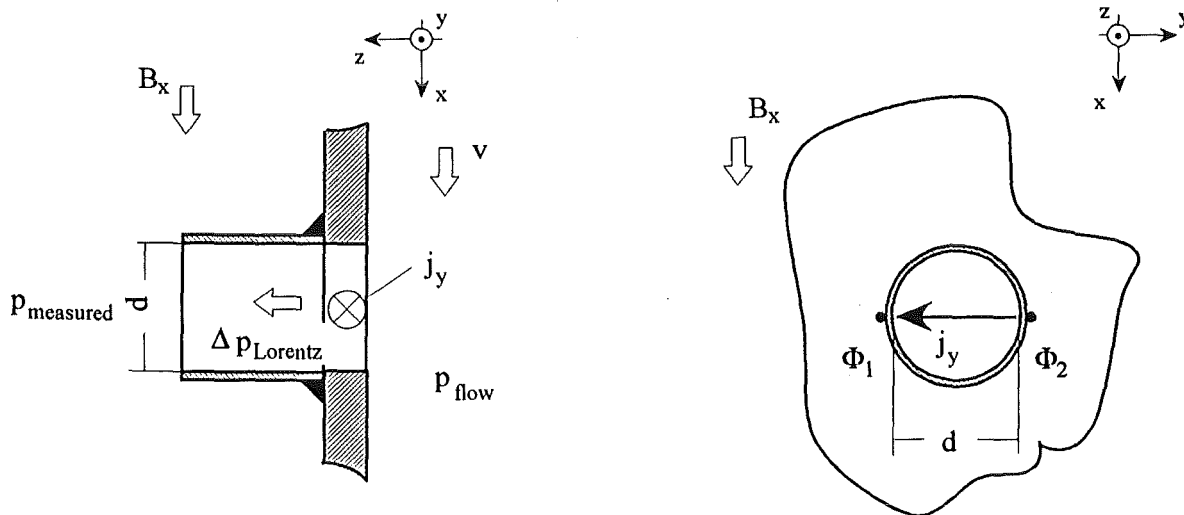


Figure 4.3 Pressure tap

The flow pattern of MHD-flows in electrically almost insulating channels ($c \ll 1$) is depicted as an electrical potential distribution on the wall. Contrary to the pressure difference measurement, the potential measurement on the channel surface has no feedback on the flow. To measure the surface potentials spring loaded needles mounted on fiberglass plates are attached to the test sections. Since the measurement is currentless the resolution of the potential measurement is only given by the resolution of the data logger.

An instrument to measure the local velocity distribution within the duct is the Liquid-metal Electromagnetic Velocimetry Instrument (LEVI) probe. It is in principle a miniaturized local electromagnetic flowmeter, see e.g. Reed & Picologlou 1986, which measures local potential gradients. The signal is proportional to the velocity and the applied external magnetic field. The velocity can be calculated according to Ohm's law:

$$\mathbf{j} = -\nabla\phi + \mathbf{v} \times \mathbf{B} . \quad (4.2)$$

One can easily see that LEVI-probes are unable to measure velocity components in magnetic field direction. The LEVI probes can be used either if the currents are known or if they are negligibly small as in almost insulating ducts at high Hartmann numbers. This limits the use of the LEVI-probe to duct flow where the condition $c \ll 1$ and $M \gg 1$ holds and where no significant three-dimensional currents circulate. In strongly three-dimensional duct flows such as radial-toroidal bends Barleon et al. 1992 have shown that LEVI probe signals may give misleading results.

Nevertheless, the LEVI is a most reliable probe, compared to hot-wire anemometers, opto-mechanical probes (Boyarevich *et al.* 1990) or temperature pulse probes (Reed & Picologlou 1986).

4.3 Data aquisition system

The data aquisition system is conducted via two independently operating personal computers which have the following tasks:

1. Control of the data aquisition hardware (Multimeters, data logger, aquisition cards, interfaces, etc.).
2. Data reduction and storage of the obtained experimental data.
3. Control of the facility.

5 Flows in hydraulic elements

Any blanket design is based on the same basic geometric elements of coolant channels. These are straight ducts of rectangular or circular cross section, expansions, contractions, bends, and manifolds. The pressure drop caused by MHD flows in these elements may be minimized by the use of thin conducting walls or by direct insulations. Flows for all these possible applications have been investigated by several authors. The main results relevant for fusion applications are summarized in the following chapters. For more detailed information the reader is advised to the original publications.

5.1 Straight duct flow

The most important duct geometries in engineering applications are straight ducts of circular or rectangular cross section. The flow in straight ducts may be either fully developed (2D) or 3D at the inlet or the exit cross sections. In very long straight ducts 3D MHD effects occur in regions of a non-uniform magnetic field or in regions of varying conductance properties of the walls, effects which are not observed in pure hydrodynamic flows.

5.1.1 Fully developed flows

Although most results for fully developed 2D MHD flows in such geometries are known for quite a long time they are repeated here for getting a complete picture. The results are summarized in the table 5.1 for thin conducting ducts with and without insulating coatings. The table shows the correlations for the pressure gradient which can be used to obtain easily results with sufficient accuracy for engineering applications. For the rectangular duct geometry the pressure gradient reaches the values of the Hartmann flow $\partial_x p_H$ if the aspect ratio b/a or the conductance ratio of the side walls c_s are large.

The sketch of velocity profiles corresponds to the position $y=0$ in the cross section. Along the y -direction the velocity is constant in the core. The no-slip condition at the wall is reached by a steep exponential decay according to equation (3.8). The velocity profile in insulating pipes takes an elliptic shape while in conducting pipes ($c \gg M^{-1}$) the flow pattern is of the slug type. Slug type velocity profiles are also obtained in the cores of rectangular ducts. However, if the duct walls are conducting the core velocity is

reduced to $v_c < 1$. The volume flux $4ab(1-v_c)$ which is now not carried by the core is carried by high-velocity jets along the side wall.

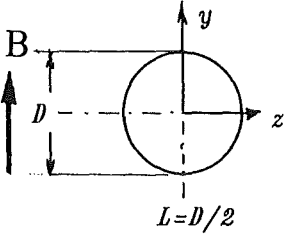
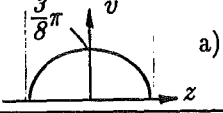
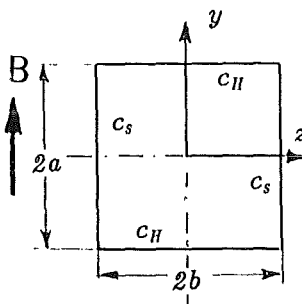
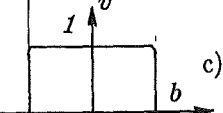
Geometry		∇p	v
 <p>$L=D/2$</p>	$\kappa=\infty$ insulating	$\frac{3\pi}{8M}$	$\frac{3}{8}\pi \cdot \sqrt{1-z^2}$  a)
	$\kappa=0$ conducting	$\frac{c}{1+c}, c \gg M^{-1}$	1
 <p>$L=a$</p>	$\kappa=\infty$ insulating	$\frac{1}{M}$	 c)
	$\kappa=0$ conducting	$\frac{\partial_x p_H}{1 + \frac{a}{3b} \frac{\partial_x p_H}{c_s}}$ where $\partial_x p_H = \frac{c_H + M^{-1}}{c_H + 1},$ $c_s^* = c_s + M^{-\frac{1}{2}}$	$v_c = \frac{\nabla p}{\partial_x p_H}$

Table 5.1 Pressure drop correlations for fully developed MHD channel flows. For details see a) Gold 1962, Shercliff 1962, b) Chang & Lundgren 1961, c) Hunt & Stewartson 1965, d) Walker 1981., Tillack 1990.

In practical applications of rectangular duct flow one will often find the more general case where the magnetic field is not aligned with any pair of walls. Results for such flows have been obtained by e.g. by Sterl 1990 on the basis of DNS or based on AM by Morley 1991, Molokov & Shisko 1993, Bühler 1994. For inclination angles $\beta > 0$ the rectangular duct splits into an inner core C_i and two outer cores C_o as shown in figure 5.1. They are separated by two thin internal viscous layers which spread from the inner corner along field lines into the fluid. The inner core exhibits a flat velocity profile while in the outer cores the velocity distribution is linear in the field direction with the highest value at the inner corner. Results for pressure drop and velocity profiles for different inclination angles β and wall conductance ratios are shown in figure 5.1.

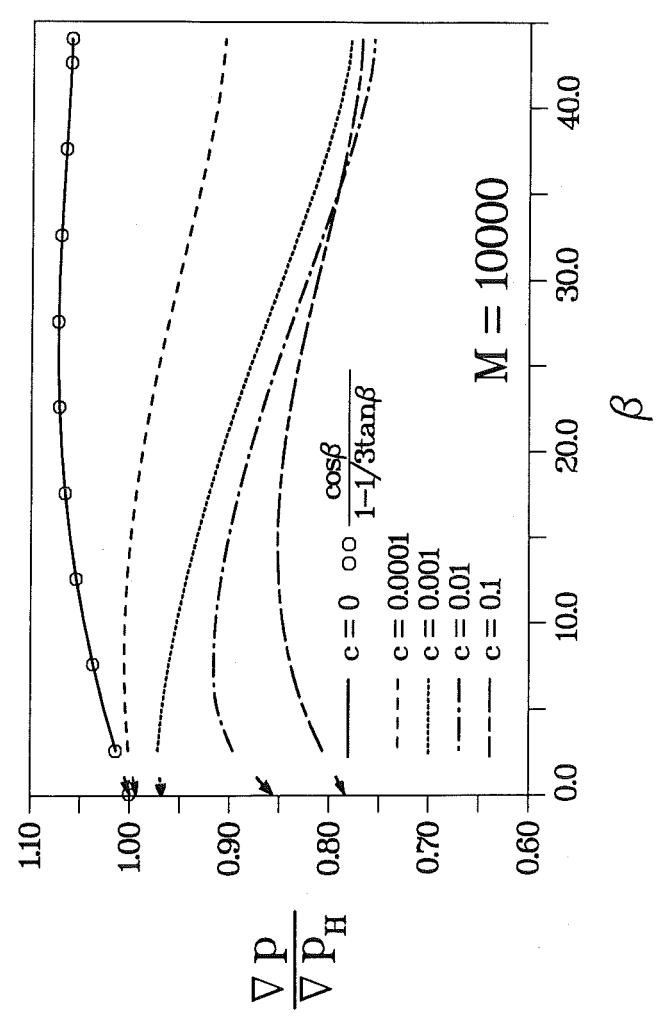
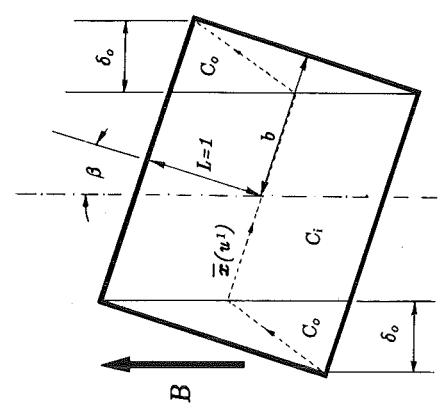
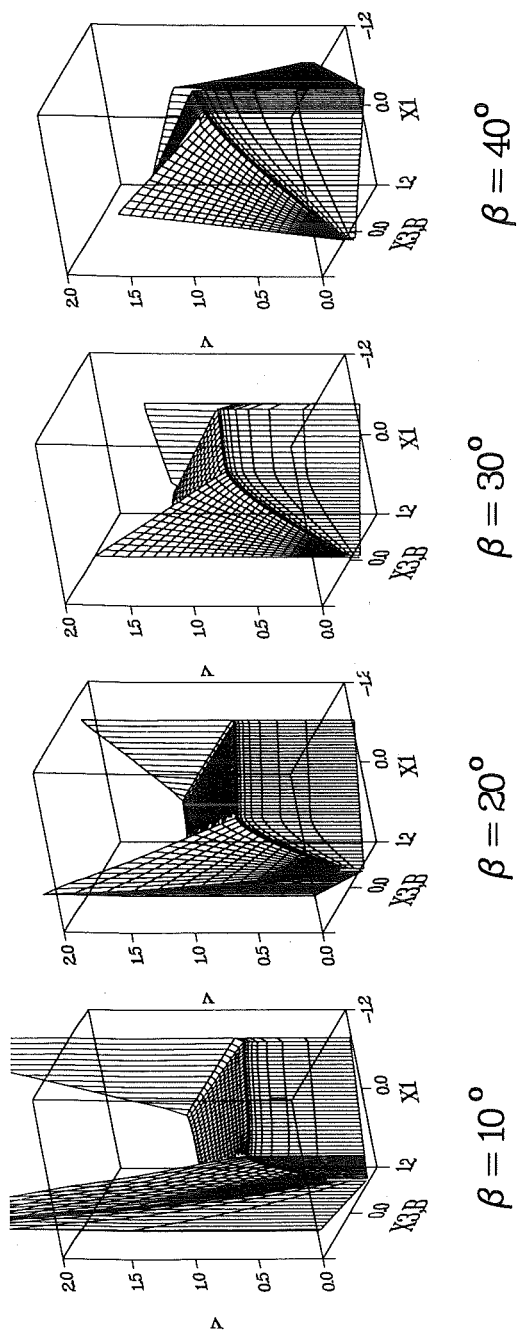


Figure 5.1 MHD flow in inclined rectangular ducts. Numerical results for velocity profiles and pressure drop (compared to the analytically obtained pressure drop $\nabla p / \nabla p_H = \cos\beta / (1 - \frac{1}{3}\tan\beta)$ obtained by Molokov & Shishko 1993 for the case $c=0$).

5.1.2 Methods for pressure drop reduction

Table 5.1 shows that the pressure drop in conducting ducts depends strongly on the wall conductance ratio c . The pressure drop may be reduced essentially if c becomes very small. Since such walls would be extremely thin they would not withstand the mechanical stresses caused by the liquid metal pressure. To overcome this difficulty the ducts with thick walls can be supplied with so-called *Flow Channel Inserts* (FCI).

A FCI consists of an insulating ceramic layer which is sandwiched between two thin steel sheets (fig. 5.2). These sheets are welded together at all edges, so that a direct contact between liquid metal and the ceramic is avoided. In contrast to direct insulating coatings the selection of the insulation material does not cause any compatibility problems with the liquid metal. FCIs are fitted loosely into the duct. Mechanical stresses are negligible because pressure equalization is possible by providing slots between the stagnant fluid in the gap and the flowing liquid metal. The pressure drop in channels equipped with FCIs is considerably reduced (Barleon *et al.* 1989) and determined by the electric resistance of the inner liner wall. Therefore, this wall should be made as thin as possible. A thickness of 0.5 mm seems sufficient for fabrication and corrosion reasons and is thin enough to reduce MHD – pressure drop to an acceptable value. The reduction of pressure drop can reach values up to 95%. The remaining pressure drop is determined by the ratio of the thickness of the inner conducting sheet and the thickness of the wall.

However, the fabrication of FCIs of large size can cause technical problems. It should be mentioned that only FCIs with a finite length, shorter than channel dimensions are possible to be produced. In this case one has to put several parts of FCIs into one channel. This can also be necessary for complex geometries. At the seam between two parts of FCIs, the liquid metal is in direct contact with the much better conducting thicker channel walls. The missing insulation in these additional seams results in a higher pressure drop. To improve this situation, an overlapping region should be used, which will reduce the additional pressure drop. A detailed analysis of this problem for a MHD flow in a circular pipe at a fusion typical high Hartmann number $M=14000$ shows that the additional pressure drop at a junction of overlapping FCIs can be reduced to a value that corresponds to the pressure drop of a fully developed pipe flow over a length of about $3.5L$ (Bühler 1993).

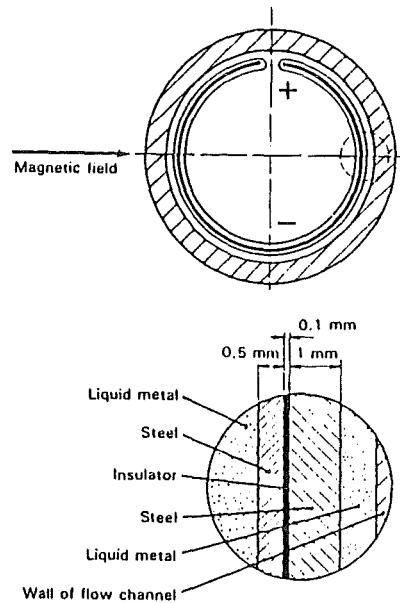


Figure 5.2 Flow channel insert (Malang *et al.* 1991).

The most efficient pressure drop reduction is obtained if the duct walls are directly covered by insulating coatings. These coatings have to withstand corrosion processes during the whole operating time of the blanket. Such insulation have been proposed by Malang 1991 and Sze *et al.* 1992. For perfect insulations $\kappa=\infty$ the pressure drop and flow pattern may be seen from Table 5.1.

If direct insulations are extremely thin ($\delta_i \ll \ll 1$) the provided coating resistance $\kappa = \rho_i \delta_i \sigma / L$ may be not sufficient to establish flow conditions like in perfectly insulating ducts. Reductions of κ may also occur during the operating time of the blanket by impurities in the insulation material, by irradiation damage or by small cracks. The influence of homogeneously reduced insulating properties on pressure drop and flow pattern has been analyzed by Bühler & Molokov (1993). Since for highly conducting ducts the reduction of the coating resistance leads to most pronounced influence on the flow this case is considered in some detail. Figure 5.3 shows the pressure gradient $\nabla p = -K$ as a function of the coating resistance. For small values of κ the pressure gradient reaches its highest value $\nabla p = -1$. For $\kappa > 1$ the pressure gradient is essentially reduced. Almost insulating conditions are reached as $\kappa \gg M$. Values of κ of $O(M)$ or smaller should be avoided in applications even if the resulting pressure drop would be acceptable because flow pattern would establish which are unfavorable for homogeneous convective heat removal.

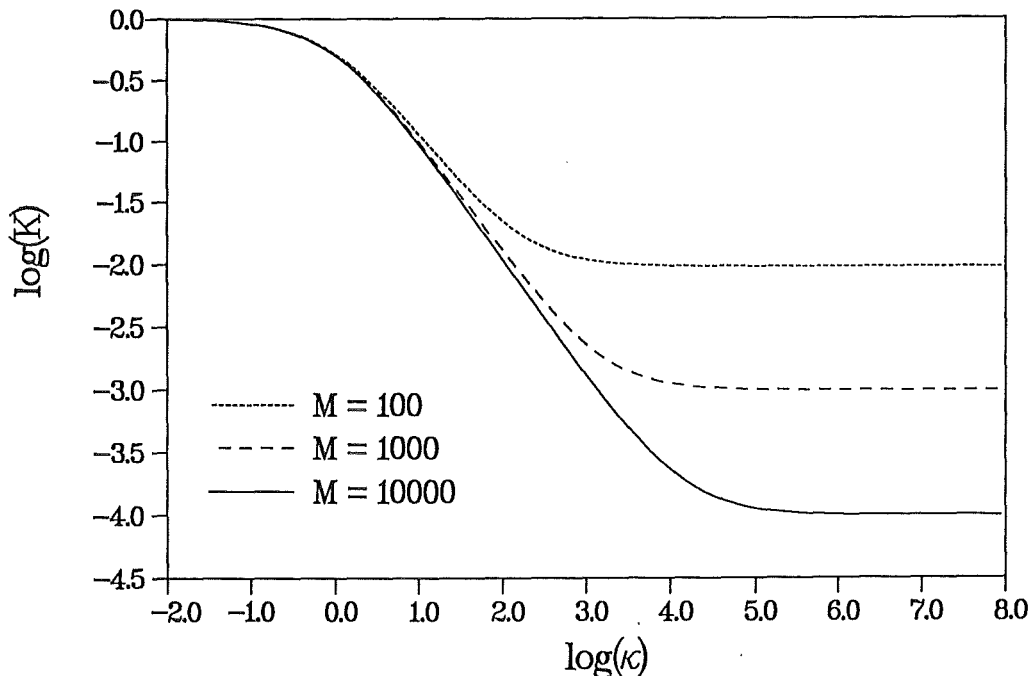


Figure 5.3 Pressure drop $\nabla p = -K$ in highly conducting rectangular ducts covered with insulating coatings (Bühler & Molokov 1993).

The influence of cracks in perfectly insulating coatings has been analyzed by Bühler (1994). The worst case with two small line cracks at both sides of the duct has been analyzed for general cross sections. For the example of circular pipe flow the cracks lead to an increase in pressure drop by a factor of about 13 compared to perfectly insulating conditions. The flow pattern shows a reversed flow near the cracks and increased velocity in the center of the duct. A 3D analysis ($M=1000$) of the flow near uninsulated small spots gives an additional pressure drop comparable to that in a perfectly insulating pipe over a length of about $25L$. The pressure and current distribution along the duct is shown in fig. 5.4. The conducting spots are at the sides $z=\pm 1$ at $x=0$.

These examples demonstrate that the number of uninsulated cracks should not exceed a certain limit. For real applications, however the situation is probably not as critical since there may exist a contact resistance at the crack, because the wall has a finite conductivity, or because of self-healing mechanisms which form a new passive layer at uninsulated parts of the channel wall.

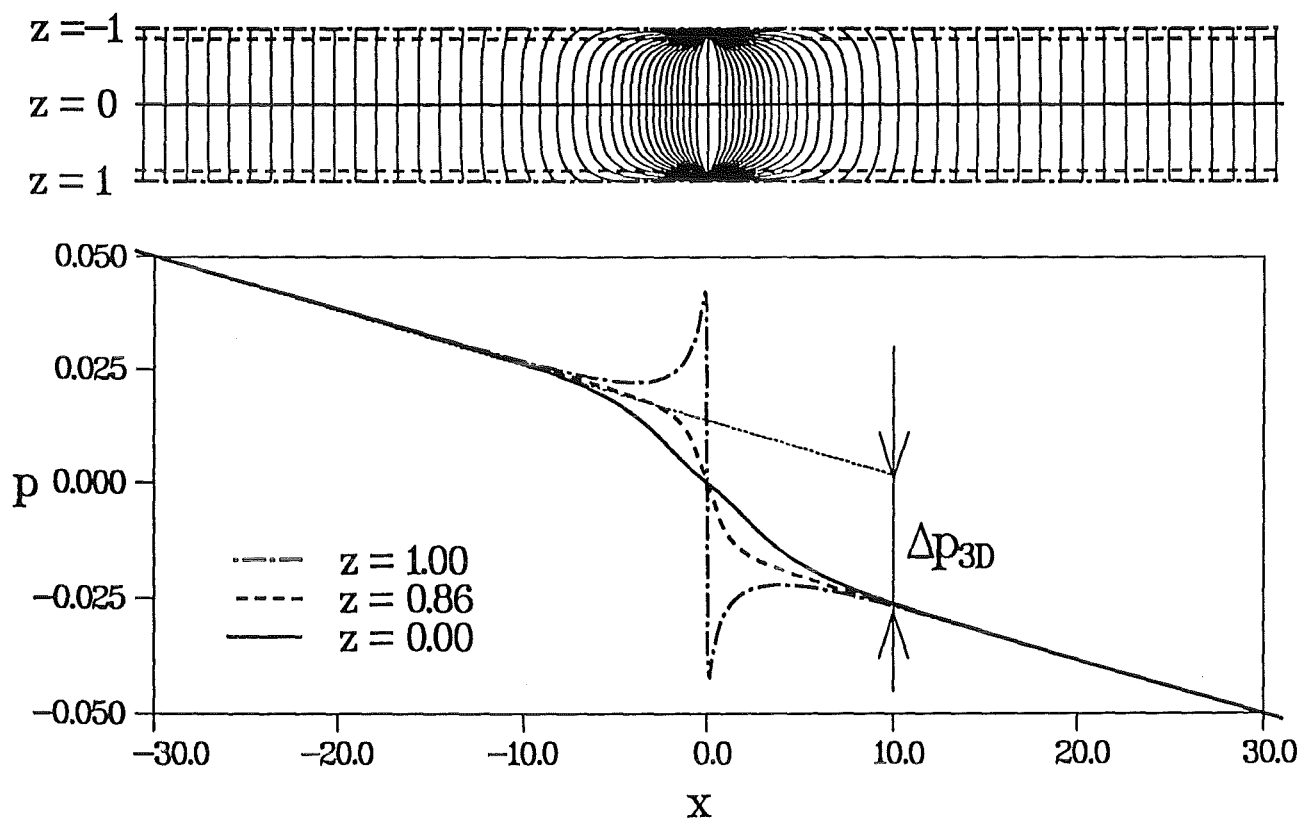


Figure 5.4 Pressure and current distribution along an insulating circular pipe with two small cracks at the sides $z = \pm 1$, $x = 0$ (Bühler 1994).

5.1.3 3D effects in straight duct flows.

The non-uniform magnetic field at the ends of the magnet causes 3D effects on pressure drop and flow pattern even in straight duct flows. The main physical reasons causing 3D effects have been already discussed in chapter 3.1 and are not repeated here.

MHD flows in fringing magnetic fields have been analyzed by DNS by several authors. The method introduced by Sterl (1990) leads to results as shown in figure 5.5. The flow with hydrodynamic velocity profile at the entrance $x=-2.13$ enters the region of the strong field downstream. Along the axis the maximum velocity in the center is reduced ($x=-0.63$), the fluid is pushed towards the side walls ($x=-0.38 \rightarrow 0.13$), and redistributed to the fully developed MHD profile at $x=2.13$. Although the Hartmann number is not extremely high ($M=50$, $N=1000$, $c=0.1$) the flow exhibits all features which occur for fusion relevant parameters. This was confirmed by Lenhart & McCarthy 1989 by a comparison of results obtained by DNS and AM. At the highest value of $M=300$ analyzed by DNS the difference with respect to results obtained by AM ($M=\infty$) reached values of only 11% for pressure drop and negligible values for core velocities. This comparison confirms both, the applicability of DNS (in conducting ducts) even if M does not reach fusion relevant values and the applicability of AM even if the Hartmann number is $M < \infty$.

A comparison (Hua & Walker 1988) of results obtained by AM for flows in a fringing field with experimental data (Reed *et al.* 1987) shows very good agreement

Results for applications described before were obtained for high interaction parameters, so that inertia effects did not play a significant role. By detailed parameter studies Lenhart (1994) finds that the dependence of the additional pressure drop $\Delta p_{3D,i}$ caused by inertial 3D effects is proportional to N^α . The exponent α which generally depends on the Hartmann number M tends towards the value $\alpha \rightarrow -1/3$ as was predicted by asymptotic theory (for other applications see Hunt & Leibovich 1967) as $M \rightarrow \infty$. At the highest investigated Hartmann number, however, this value has not been reached yet.

AM for calculating flows in straight pipes of circular cross section have been introduced for conducting walls by Talmage & Walker 1987. Barleon *et al.* 1989 compared results obtained by the same approach with experimental data and found excellent agreement (see fig. 5.6). Flows in insulating pipes have been analyzed by Hua & Walker 1989. The common result of all these works is, that in the fringing field region the velocity in the 3D region is reduced in the center of the duct and more fluid is pushed towards the sides. Behind the 3D region the fluid is redistributed to fully

developed conditions. The strong 3D effects result in an additional pressure drop Δp_{3D} . This pressure drop can not be expressed by simple empirical formulas because it depends not only on conductance properties of the walls but in addition on the variation of the magnetic field, which is different in several applications. The results, however, show that the AM are appropriate methods for the calculation of 3D effects on pressure drop and flow pattern in a fringing field.

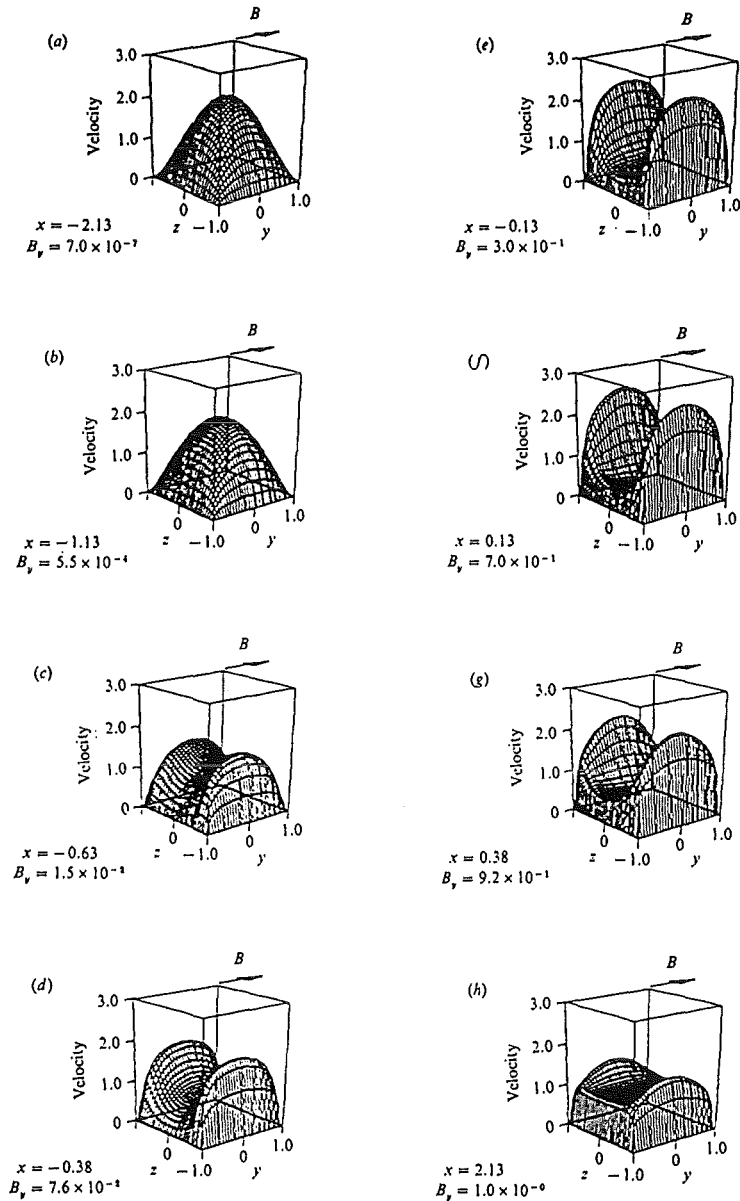


Figure 5.5 Profiles of axial velocity in the entrance region of a magnet at different cross-sections. Starting from the fully developed hydrodynamic flow the velocity is redistributed in the transition region, the fluid being driven towards the side walls. The evolving M-shaped profile then decays into the fully developed MHD profile. (Sterl 1990).

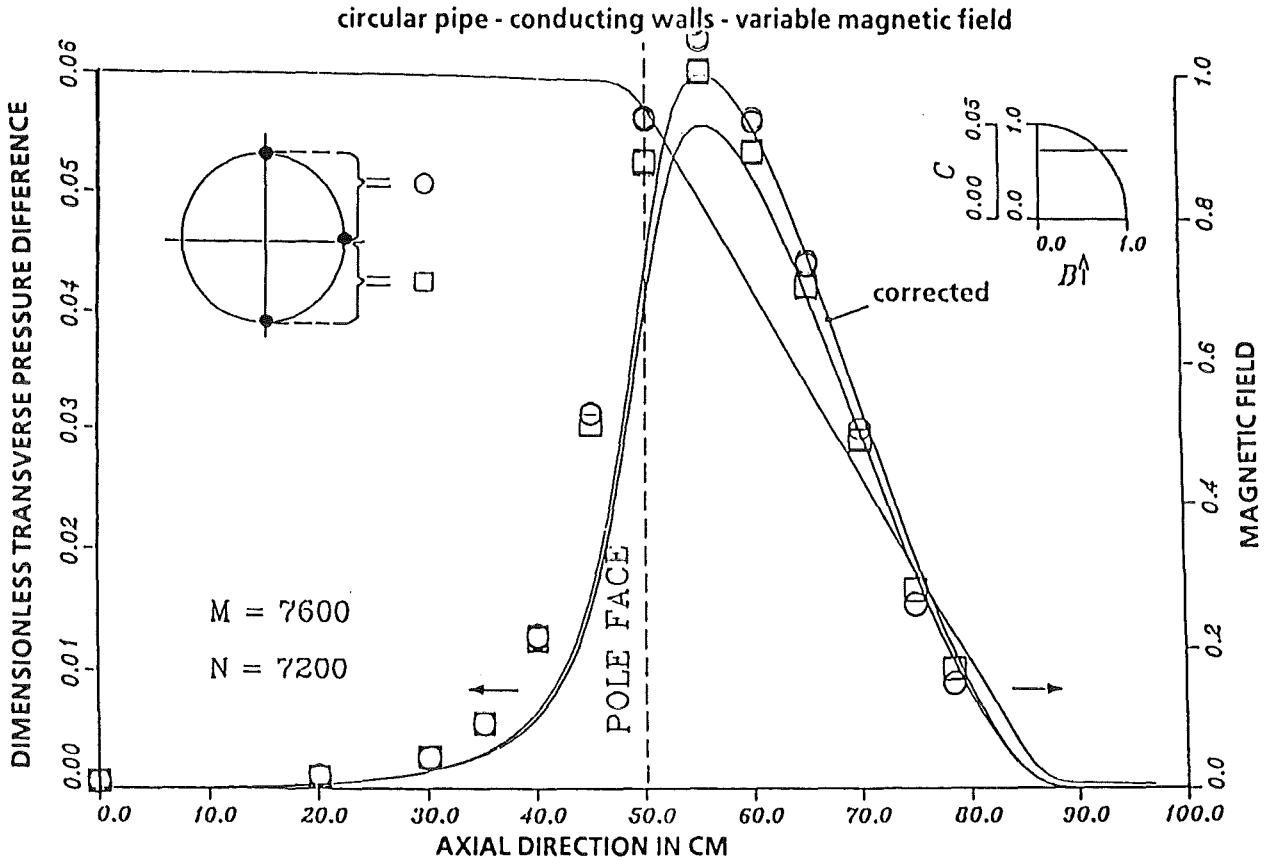


Figure 5.5 Transverse pressure difference for circular pipe flow in a fringing magnetic field. Comparison of experimental data and asymptotic theory (Barleon 1989).

5.2 Variable cross section area

In real engineering applications straight ducts of different size or shape have to be connected to the global coolant loop system. 3D geometries like expansions, contractions or other complex types are unavoidable.

5.2.1 Expansions, contractions

Since expansions or contractions may have a strong influence on pressure drop and flow distribution MHD flows in such geometries have been analyzed by a number of authors (e.g. Hunt & Leibovich 1967, Walker & Ludford 1974, McCarthy, K.A. 1989, etc.). All their results show the common feature, that if the flow expands in the field direction all effects are comparable to those in a fringing field. The influence on pressure drop and flow pattern is most pronounced. Here an example of an MHD flow in a circular expansion for $M=1000$ is presented. The strongest influence is observed in insulating ducts as shown in figure 5.7. The cross section expands monotonically and smoothly from $r=1$ at $x \leq -2$ to $r=2$ at $x \geq 2$. In the expanding part the fluid velocity is essentially reduced in the center and displaced towards the sides. The development length is of the order \sqrt{M} (Walker & Ludford 1974) so that at $x=7 < \sqrt{M}$ the flow is still far from being fully developed. The fully developed conditions $\nabla p = -3\pi/8M$, $v = \sqrt{1-z^2}3\pi/8$ at the entrance as $x \ll -\sqrt{M}$ and $\nabla p = -3\pi/32M$, $v = \sqrt{1-\frac{1}{4}z^2}3\pi/32$ at the exit as $x \gg \sqrt{M}$ are reached. The irreversibly lost amount of pressure drop is Δp_{3D} .

The influence of the wall conductance ratio on MHD flows in non-insulating circular expansions have been analyzed in detail. The additional pressure drop is compared to the pressure drop in a circular pipe (entrance cross section) over the equivalent length l_{3D} . The results plotted in figure 5.8 show that 3D effects (l_{3D}) caused by 3D electric currents vanish as the wall is perfectly conducting ($c \rightarrow \infty$) since all currents close their circuit in the walls and not inside the fluid. As $c \rightarrow 0$ the flow behaves like in insulating expansions. Although the 3D effect is most pronounced (maximum value of l_{3D}) the total pressure drop is still acceptable.

Similar results have been obtained for flows in expansions of rectangular cross section (Burr & Bühler 1994). While in ducts with expansions in the field direction only the influence is even stronger than in circular ducts (see Figure 5.9). 3D effects become almost negligible if the expansion occurs only in the plane perpendicular to the field. The difference between both types of expansions is outlined by some simple considerations.

The transverse potential difference $\Delta\phi \sim b \cdot \bar{v}$ in poorly conducting ducts is proportional to the product of the duct width b and the mean velocity $\bar{v} \sim 1/ab$. Therefore it is obvious that an axial potential gradient $\partial_x \Delta\phi$ responsible for 3D effects is established only if there is a variation of a , the dimension in the field direction, with x . Variations of b do not cause significant 3D effects.

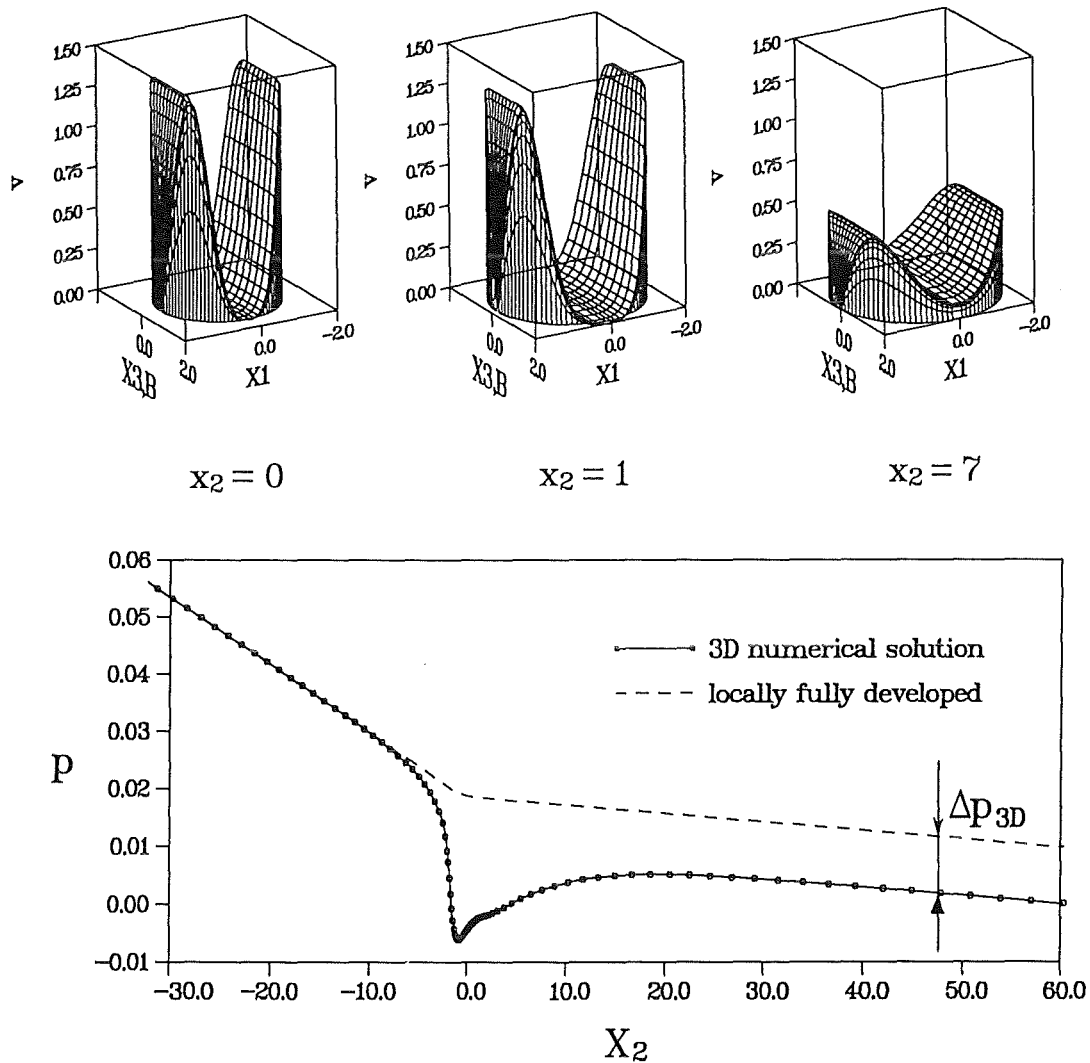


Figure 5.7 MHD flow in an insulating circular expansion at $M=1000$. $r(x_2 < -2) = 1$, $r(x_2 > -2) = 2$. Flow pattern and pressure distribution along the axis (Bühler 1994).

These considerations show that variations of the cross section should occur only in the plane perpendicular to the field in order to avoid higher pressure drop caused by 3D effects. All results obtained for flows at high interaction parameters in expanding geometries are directly valid for contracting geometries as well since the flow problem becomes linear.

A geometry of periodically varying cross section has been designed and investigated theoretically and experimentally, called the *Flow Tailoring Testsection*. The aim of these investigations was to allow some additional pressure losses due to 3D effects, but to take more profit in heat transfer enhancement by the high velocity 3D flow pattern. The agreement between AM-results and experimental findings presented by Picologlou *et al.* 1989 is very good.

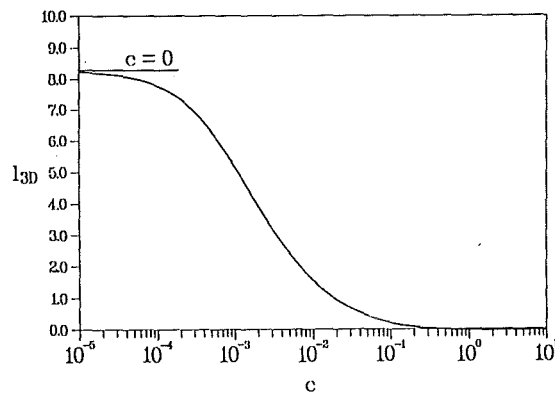


Figure 5.8 Additional pressure drop in a conducting circular expansion compared to the equivalent length l_{3D} of a fully developed pipe flow as a function of the wall conductance ratio. ($M=1000$). (Burr & Bühler 1994).

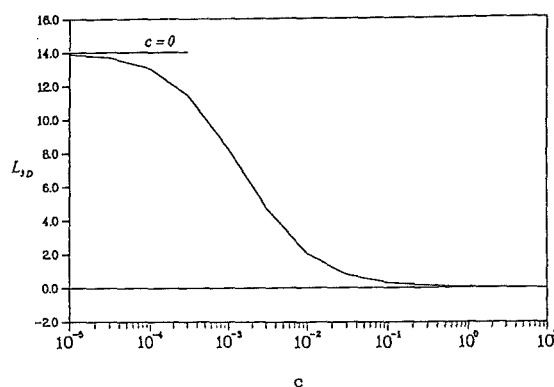


Figure 5.9 Additional pressure drop in a conducting rectangular expansion in the plane of the field compared to the equivalent length l_{3D} of a fully developed duct flow as a function of the wall conductance ratio. ($M=1000$). (Burr & Bühler 1994).

5.2.2 Flow in a complex geometry of a blanket element

The MHD-flow in the poloidal collector of a blanket is investigated next. The geometry shown in figure 5.10 is exactly related to the geometry of the *Dual Coolant Concept* (Malang *et al.* 1993), but is considered here to have thin conducting walls. The flat rectangular channel has already collected the flow rates from the poloidal sub-channels. The fluid flows further through an expansion region at the end of which the cross section is almost of square shape. The last rectangular cross section is connected with the circular pipe by a smooth transition zone. All flow variables and non-dimensional parameters are scaled with the pipe radius as the characteristic dimension. The wall-conductance ratio and the Hartmann number have been chosen to be $c=0.05$ and $M=10^4$, respectively. Figure 5.10 shows isolines of wall potential plotted on the surface of the duct. The diagram shows the variation of pressure along the axis.

When the fluid passes through the expansion region it is not subjected to significant 3D-effects. The expansion has been designed with an optimal orientation. The flow expands only in the plane perpendicular to the magnetic field. The extension in the field direction has been kept constant. Due to the reduction of the velocity, the pressure drop decreases in the expanding region. At the junction between the rectangular duct and the circular pipe 3D-effects are unavoidable. They cause there an irreversible pressure drop Δp_{3D} , as indicated in the diagram. Δp_{3D} is equivalent to the pressure drop in the circular pipe, estimated over a length of about $l_{3D} \approx 0.6$. A comparison with the total height of the blanket shows that this is still a relatively small amount. In the circular pipe the fully-developed pressure gradient of $\nabla p = -c/(1+c)$ is reached very quickly in a short distance.

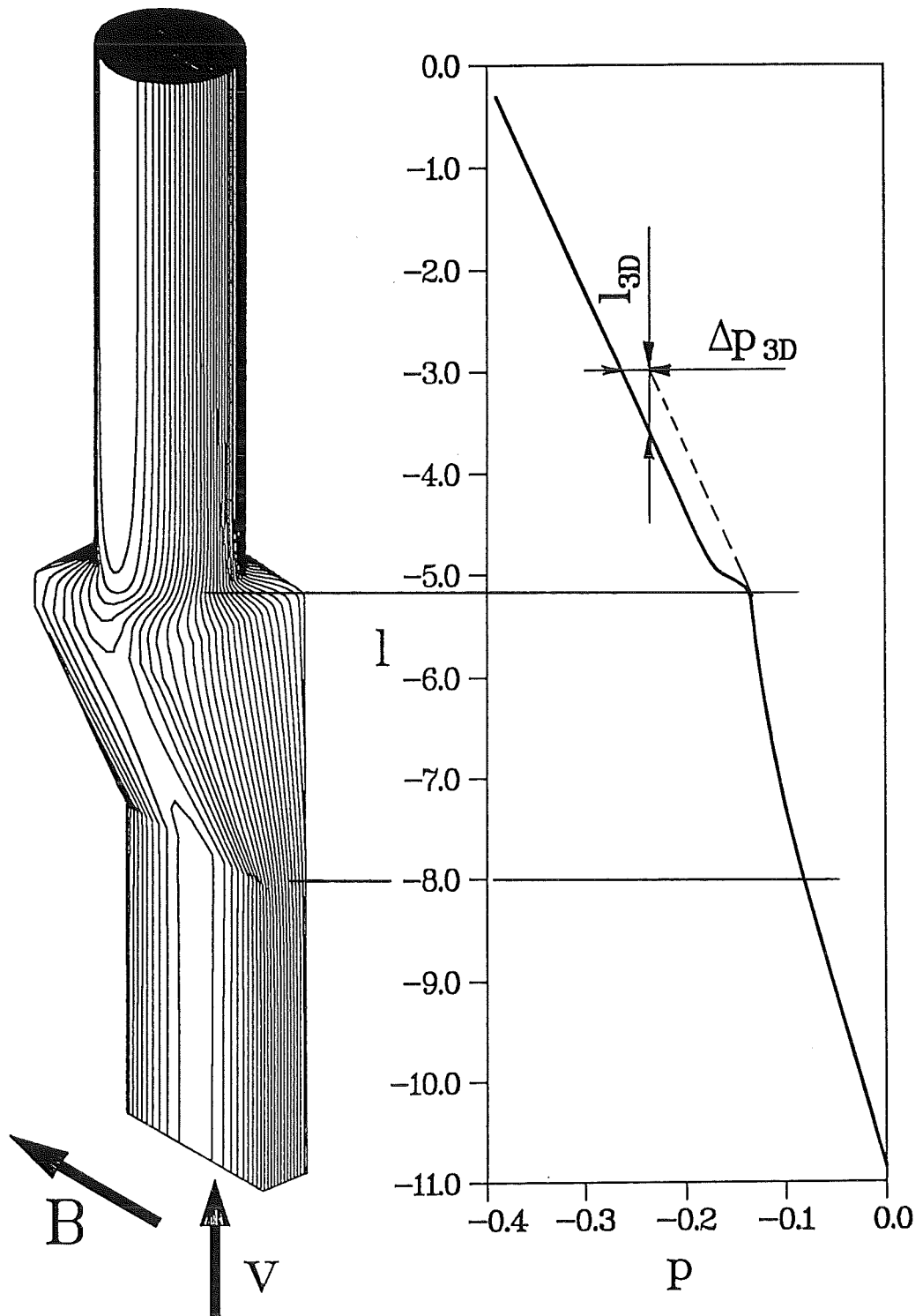


Figure 5.10

3D MHD flow in a complex element of a recently designed fusion blanket. $M=10000$, $c=0.05$. Lines of constant wall potential on the surface of the duct, variation of pressure along the axial coordinate. (Bühler 1994).

5.3 Bends

Other important elements in fusion reactor blankets are bends which turn the coolant from downward poloidal flow to upward poloidal flow (see the blanket concepts described by Malang *et al.* 1988, or Malang *et al.* 1993) or from poloidal to radial or from radial to toroidal direction (Malang *et al.* 1988). The first type of bends turn the fluid motion in the plane perpendicular to the magnetic field direction, while the latter changes the flow direction from a direction perpendicular to B into a direction perfectly aligned with B . The flow in both types of bends will be analyzed and discussed in the following sections.

5.3.1 Bends in the plane perpendicular to the magnetic field

Flows in electrically conducting bends in the plane perpendicular to the field have been analyzed by Walker (1986). He did not find a significant increase in pressure drop due to 3D effects. In his analysis of flows in conducting bends of circular cross section he found the pressure drop to be comparable to that in a straight pipe of the same mean length. The reason for negligible 3D pressure drop can be explained by the same arguments as before for the expansion in the plane perpendicular to the field since the cross section changes only in this plane. Although there is almost no increase in pressure drop the flow patterns in the bend cross sections are significantly changed. At the inner radius of the bend the velocity is increased, whereas at the outer radius of the bend the velocity is decreased.

More interesting for fusion applications are bends of rectangular cross section. Results obtained by AM (Bühler 1994) are plotted in figure 5.11. They show the same tendency as Walker's results described above. The flow enters and leaves the computational domain with the fully developed MHD velocity profile which exhibits a flat core and two high-velocity jets along the side walls. In the bend the velocities near the inner radius are increased, those near the outer side wall are decreased, in the core as well as in the side layers. An increase of pressure drop compared to that of a straight duct flow along the same mean length can not be found.

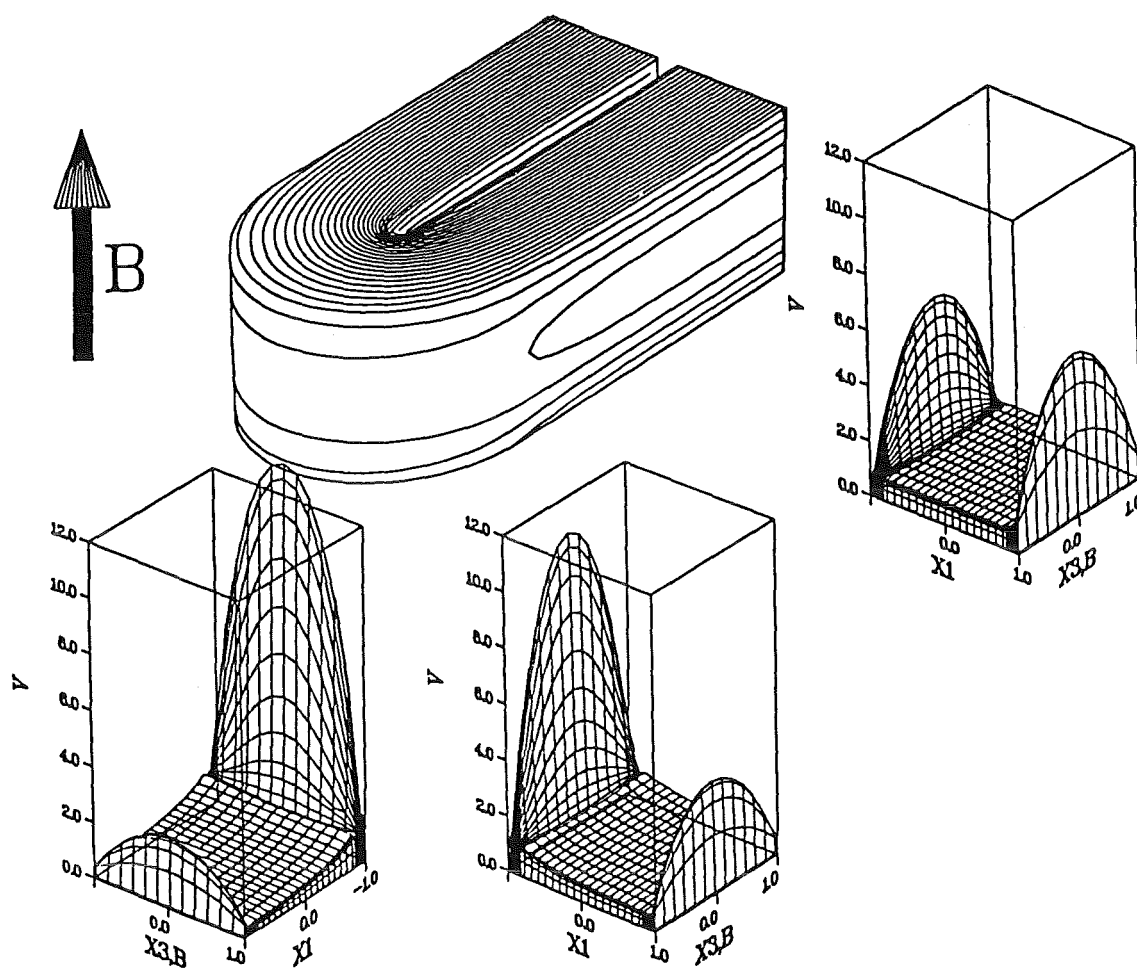


Figure 5.11 3D MHD flow in a bend in the plane perpendicular to the field. Lines of constant potential on the surface of the duct and three velocity profiles at different axial positions.

5.3.2 Bends in the plane of the magnetic field

More significant are bend flows which turn the flow from a direction perpendicular to the field into a direction aligned with the field. In the blanket concept described by Malang *et al.* 1988, there are two bends forming an U-bend with radial-toroidal-radial orientation. Since in the toroidal part which is perfectly aligned with the magnetic field the main flow direction coincides with the direction of the field the induced potential in this duct is zero. This part of the bend therefore serves as an additional current path and increases the total current and pressure drop in the radial leg. We consider here only one

half of the U-bend (see figure 5.12) with appropriate boundary and symmetry conditions. In the toroidal plane of symmetry $y=y_s$, the symmetry conditions for the leading variables used in the analysis are

$$p = 0, \quad \phi = 0 \quad \text{at } y_s. \quad (5.1)$$

If the toroidal duct is long enough $y_s \rightarrow \infty$ the resulting flow should approximate the flow near the junction in a single 90° bend. At large distance from the bend in the radial direction the flow should be fully developed.

$$\frac{\partial p}{\partial x} = \text{const}, \quad \frac{\partial \phi}{\partial x} = 0. \quad \text{as } x \rightarrow \infty. \quad (5.2)$$

The detailed analysis of this problem based on AM is described by Molokov & Bühler 1994.

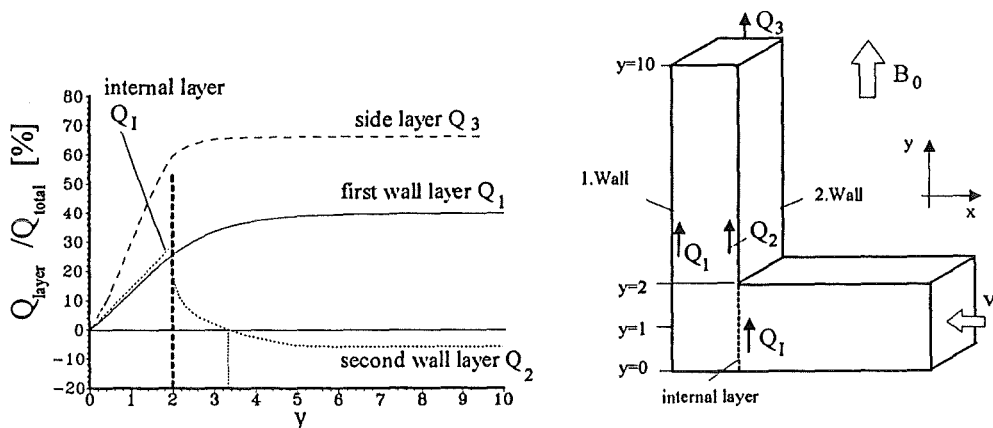


Figure 5.12 Flow rates in the wall-adjacent boundary layers in the toroidal duct. Sketch of geometry, orientation of the magnetic field, and coordinates. $M=\infty$, $c=0.052$. (Stieglitz 1994).

Here only the main results are summarized.

- The core of the toroidal duct has no component of velocity in the main toroidal direction.
- The flow in the toroidal duct is confined to thin boundary layers at all walls which are aligned with the field and which carry all flow rates Q_i . Even at the first wall there is a jet which carries a significant rate Q_1 of the total volume flux. The variations of flow rates in the layers along the toroidal coordinate y are shown in figure 5.12. At $y > 3.3$ the flow in the second wall layer becomes reversed because of the strong pumping and mass exchange via the toroidal core.

- The core in the toroidal duct is by no means stagnant. There is an intense exchange of fluid between the four layers which are aligned with the field. This exchange happens because of a direct interaction between neighboring layers or even along larger distances if the core is involved. There is fluid motion in the core only in planes $y=const$, and it does not contribute to an $O(1)$ volume flux in the toroidal direction. Nevertheless, this motion may lead to improved heat transfer conditions. The intensity of the flow in the core is most pronounced at the Hartmann wall of the toroidal duct and vanishes at the plane of symmetry. The flow behaves qualitatively like the flow analyzed by Molokov & Bühler 1994, shown in figure 5.13.

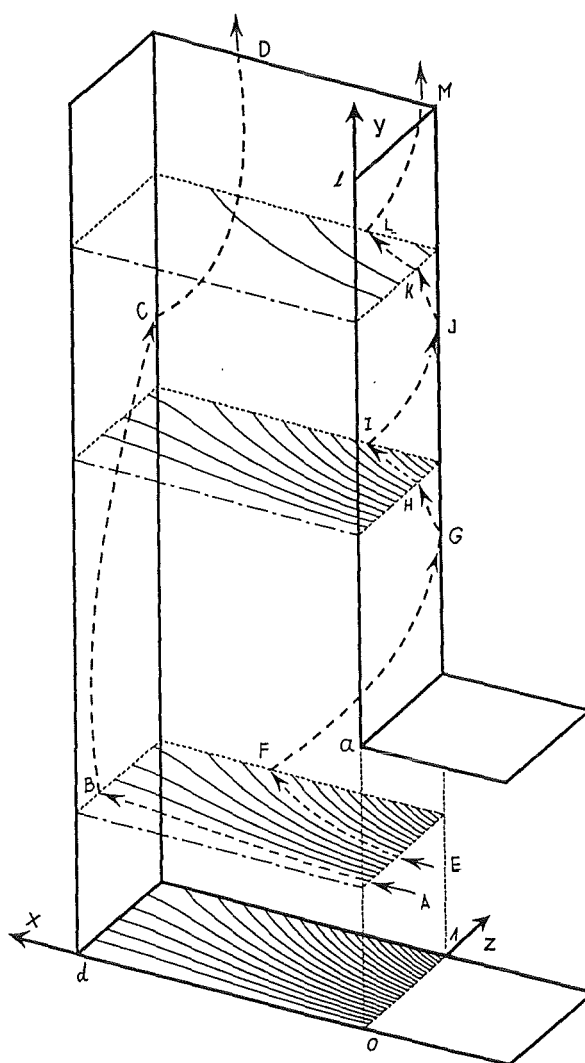


Figure 5.13

Isolines of potential at the bottom of the toroidal duct, streamlines in the toroidal core and sketch of flow path in the layers. (Molokov & Bühler 1994)

The flow in the radial toroidal bend has been intensively investigated experimentally (Stieglitz 1994) and compared with AM—results. The wall conductance ratio used in the experiment and in the analysis was $c=0.052$. The main results are summarized next:

I. Wall potentials: Wall potentials have been measured at the positions A–Q. The distances between their positions and the outer corner are shown in dimensionless scale in fig. 5.14. Only potential distributions at characteristic positions, along fat—solid lines, marked by the bigger letters are discussed below. The others, along thin—solid lines show quite the same tendency.

The measured values of the wall potential at different positions are shown for a relatively low interaction parameter $N=1995$ in figure 5.15 for a wide range of Hartmann numbers $M=1937-8177$. They are compared with the calculated potential distributions shown as solid lines.

The excellent agreement of measured and calculated values of potential at the position A confirms the assumption of fully developed MHD flow, used as a boundary condition for calculation. A variation of the Hartmann number at positions A,E,J does not have an influence on the wall potential indicating that even flows at the lowest investigated Hartmann number $M=1937$ exhibit the asymptotic distribution of the wall potential, in good agreement with the theory.

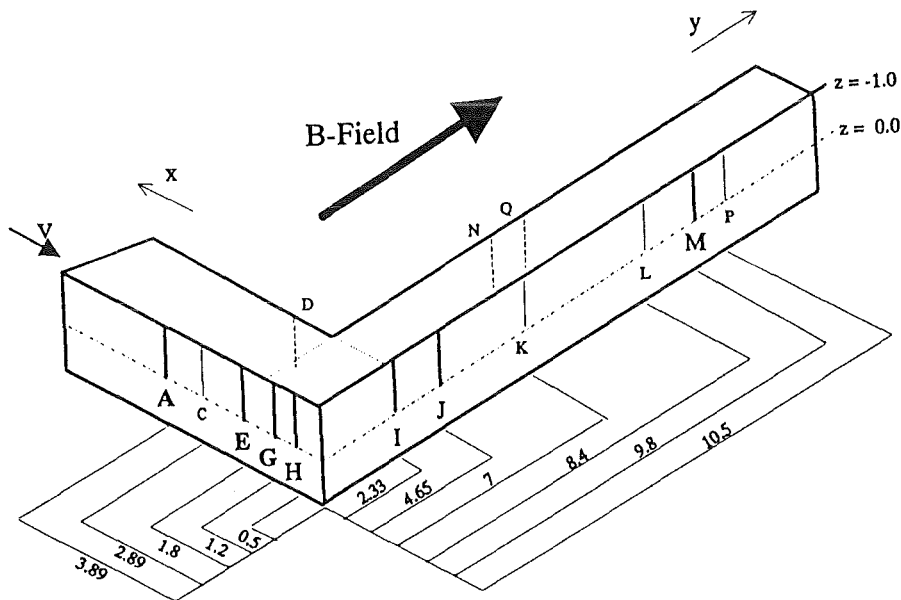


Figure 5.14 Positions where wall potentials are measured. At the Hartmann wall of the radial duct (A–E), at the Hartmann wall of the toroidal duct (G,H), at the first wall (I–M). (Stieglitz 1994).

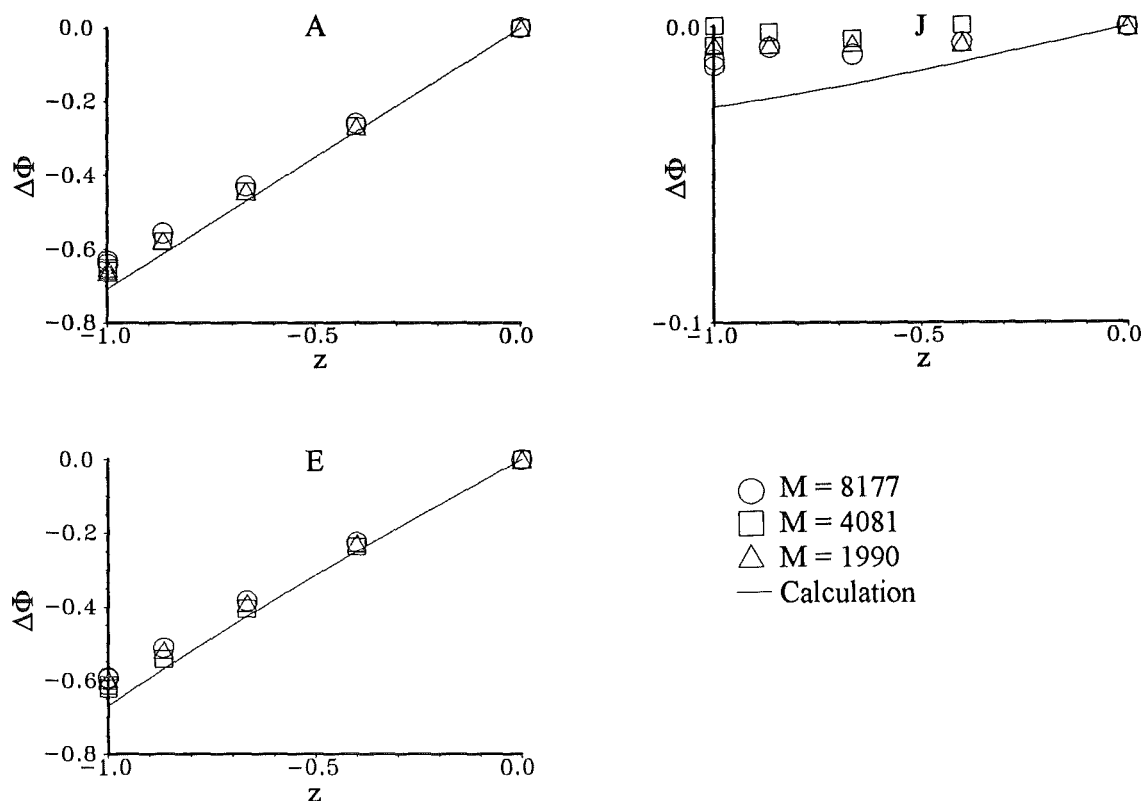


Figure 5.15 Wall potentials at the positions A,E,J for different values of the Hartmann number M at an interaction parameter $N=1995$, compared to the asymptotic theory $N, M \rightarrow \infty$. (Stieglitz 1994).

The influence of inertial effects was expected to have a significant effect on the wall potential in the vicinity of the bend where the main flow direction changes. Measured potentials at a high Hartmann number, $M=7984$, and for interaction parameters in the range of $1995 < N < 27340$ are compared with the calculated values in figure 5.16. The experimental data do not show a significant dependence on N since all measured values are spread only over a small range, which actually represents the experimental accuracy. Even bend flows at the lowest investigated interaction parameter $N=1995$ show the asymptotic values of the wall potential. Small differences of measured and calculated potentials at positions G and H occur only close to the side wall ($z=-1$). Even at position I the agreement between experiment and theory is surprisingly good, although one would expect there some discrepancies caused by inertial effects. A more pronounced dependence of the wall potential on the interaction parameter N is obtained at the side walls of the toroidal duct (see figure 5.17). For increasing N the experimental data tend towards the calculated values of inertialess bend flow.

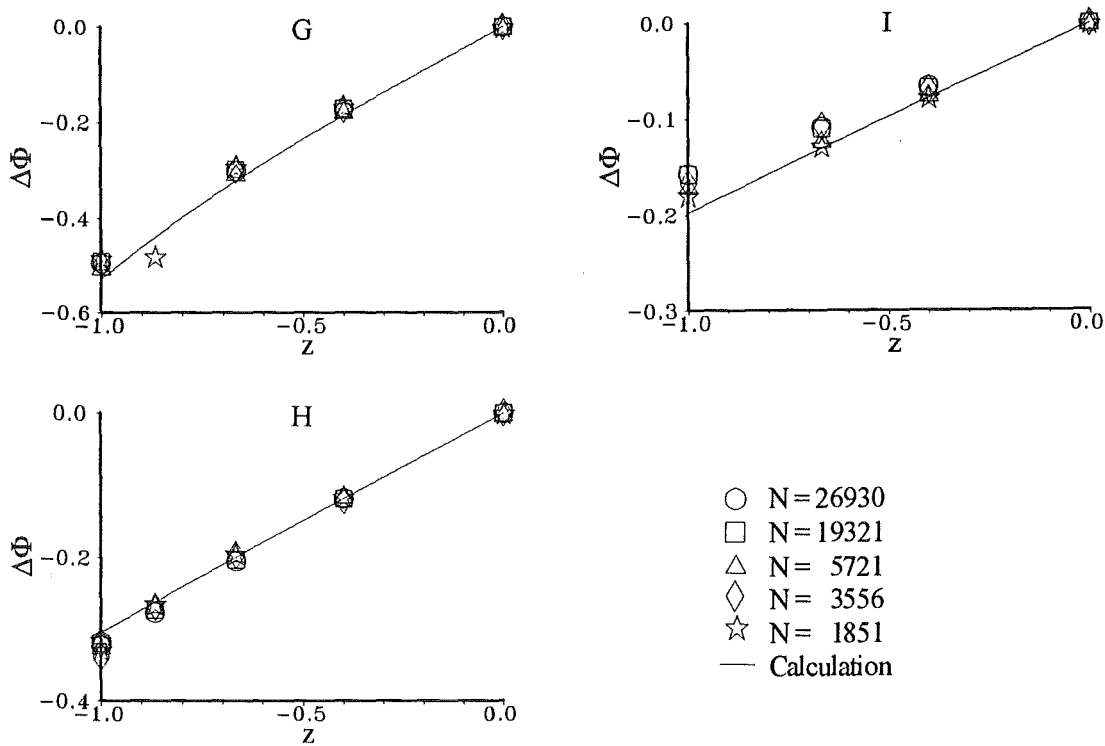


Figure 5.16 Wall potentials at the positions G, H, I for different values of the interaction parameter N at a Hartmann number $M=7984$, compared to the asymptotic theory $N, M \rightarrow \infty$. (Stieglitz 1994).

II. Pressure: Values of pressure drop have been measured between several positions along the outer wall of the bend in the plane of symmetry as shown in figure 5.18.

The inlet boundary condition used for calculations may be checked by a comparison of the measured pressure difference between the positions $D3$ and $D4$ with the pressure drop of a fully developed MHD flow. Figure 5.18a indicates that for a Hartmann number $M=8000$ the experimentally employed length of the radial duct provides fully developed conditions between the positions $D3$ and $D4$ only for high interaction parameters N . For lower values of N additional 3D effects give a noticeable contribution to the pressure drop. This effect is independent of the flow direction an observation which may be explained by the symmetry of the Z-bend used in the experiment.

In the asymptotic limit of the basic equations the pressure should not vary along magnetic field lines. However, this condition could not be satisfied perfectly during the experiment. The pressure differences $D5-D6$ (figure 5.18c) or $D7-D9$ (figure 5.18d) result from the small normal magnetic field component at the first wall due to the

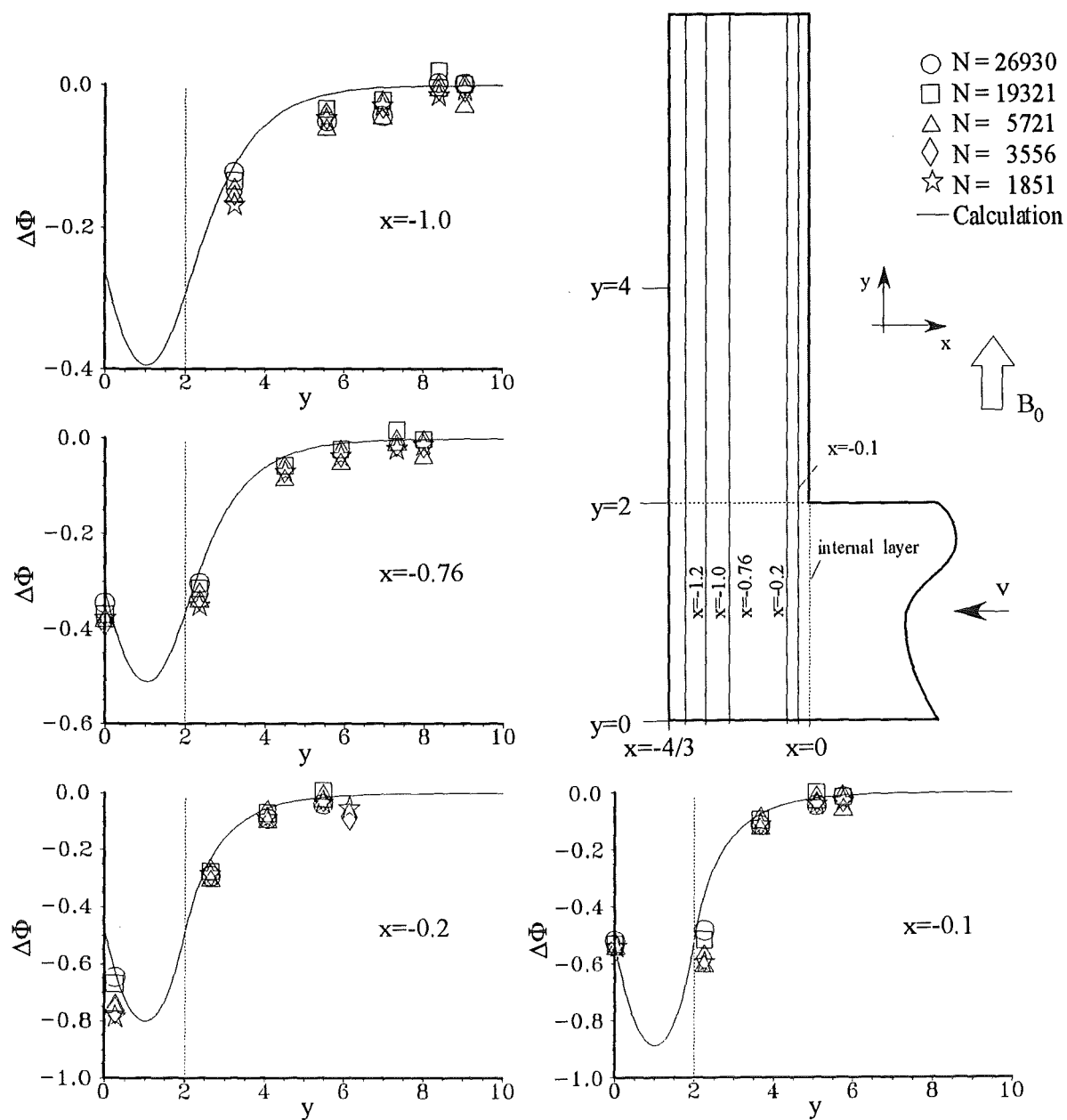


Fig. 5.17

Wall potentials at the positions $x = -1.2 - 0.2$ for different values of the interaction parameter N at a Hartmann number $M = 8177$, compared to the asymptotic theory $N, M \rightarrow \infty$. (Stieglitz 1994).

inhomogeneity of the experimental field.

Figure 5.18e shows experimental values of the total pressure drop over the whole bend. The calculated asymptotic limit is confirmed almost exactly by the experiment for high values of N . For $N < 2000$ the total pressure drop shows a significant dependence on N and M , which may be fitted by the following correlation:

$$\Delta p_{tot.} = \Delta p_{asympt.} + 0.406 \cdot N^{-0.337} + 0.939 \cdot M^{-0.565}. \quad (5.3)$$

The expression (5.3) has been obtained by a statistical analysis of the experimental data. The exponents -0.337 and -0.565 are very close to theoretically predicted values $-1/3$ and $-1/2$, respectively. This means that in the inertial flow regime the layers are characterized by inertial–electromagnetic interaction.

The asymptotic value $\Delta p_{asympt.}$ for high M and N may be split in a part of fully developed MHD flow perpendicular to the field and an additional contribution of inertialess 3D effects.

$$\Delta p_{asympt.} = \Delta p_{fd} + \Delta p_{3D}, \quad (5.4)$$

or

$$\Delta p_{asympt.} = (l_{rad} + l_{3D}) \left. \frac{\partial p}{\partial x} \right|_{fd}. \quad (5.5)$$

The equivalent length l_{3D} characterizing the additional pressure drop Δp_{3D} in the considered bend flow is $l_{3D} = 0.563$, which is for sure not critical for blanket applications. l_{rad} is the length of the radial duct. Since some blanket elements require flows with $N < 2000$, equation (5.3) can be used as inertial correction to the theoretically obtained asymptotic solution for pressure drop.

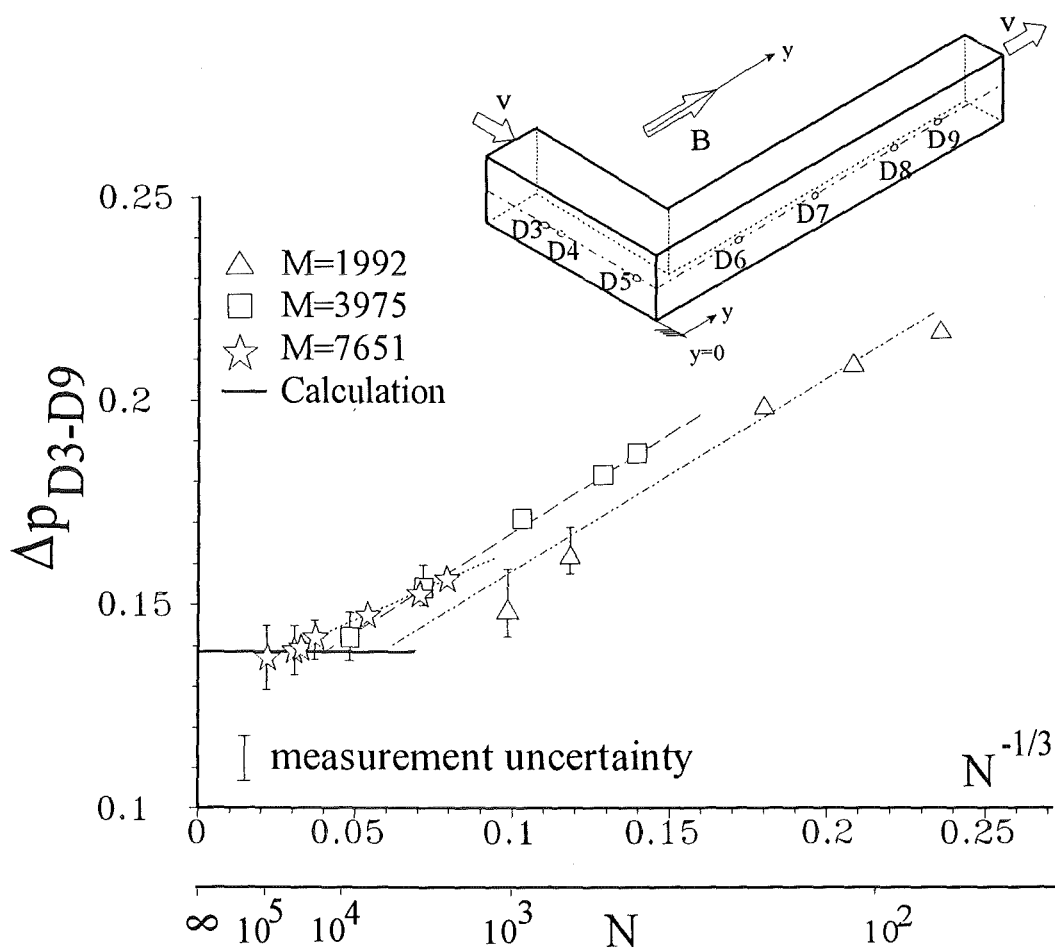
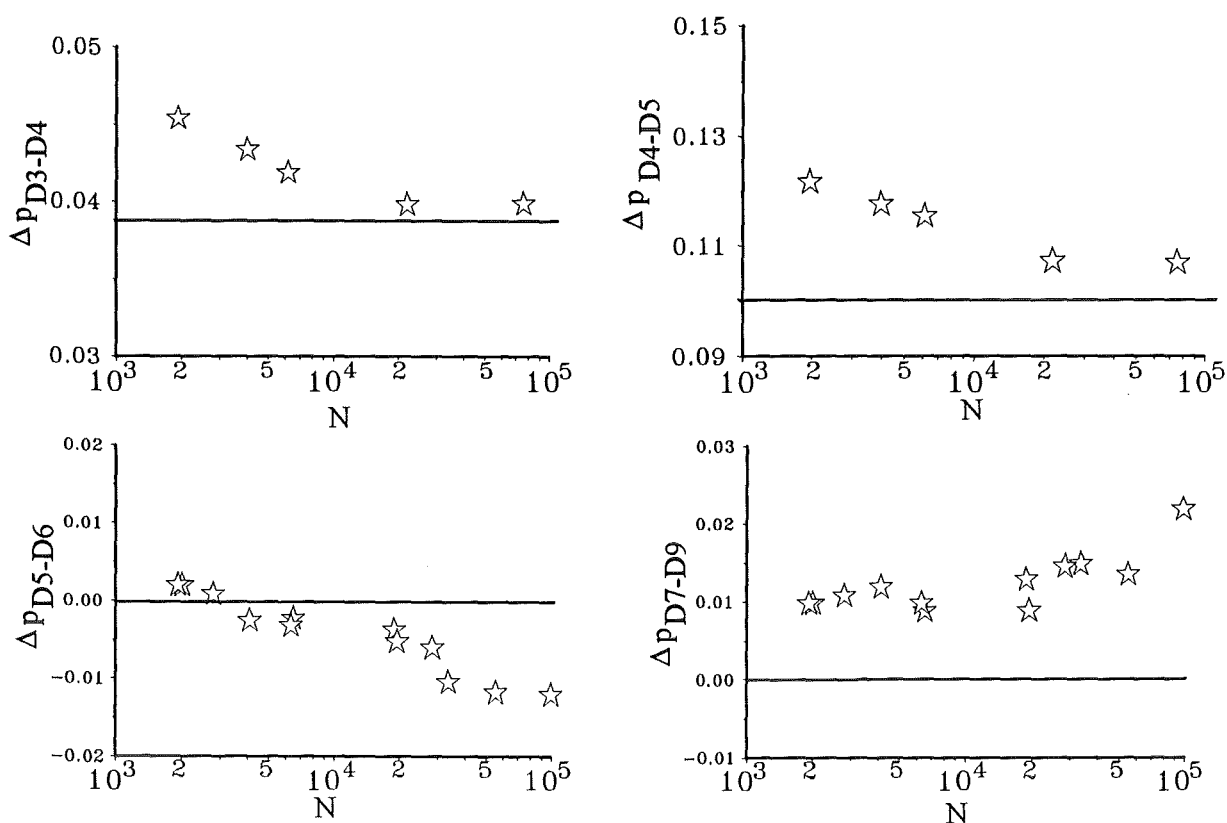


Figure 5.18 Pressure differences between several positions $D3-D9$ for different values of the interaction parameter N at a Hartmann number $M=7984$, compared to the asymptotic theory $N, M \rightarrow \infty$.

III. Sensitivity to small inclinations: In real engineering applications the desirable perfect alignment of the toroidal duct walls with the magnetic field can not be achieved. To investigate the effect of small inclinations with respect to the magnetic field direction the test section was turned in the experiment by small angles. The maximum angles of inclination with respect to a rotation around the z -axis were limited by the test volume of the used magnet to $-5^\circ < \Theta_z < 15^\circ$ (see figure 5.19). Figure 5.19 shows the total pressure drop for the three angles $\Theta_z = -5^\circ, 0^\circ, 15^\circ$ as a function of the interaction parameter N . For high values of N the pressure drop caused by the flow with the three orientations is almost the same. For small values of N the pressure drop in bends with $\Theta_z = -5^\circ$ and $\Theta_z = 0^\circ$ is still comparable, but significantly different from the case of $\Theta_z = 15^\circ$, for which it is about 30% higher. The reason for higher pressure drop in the latter case can be explained by the internal layer (*Ludford layer*) which occurs at the inner corner of the bend along field lines. This layer carries a significant amount of the total flow rate in a thin, high-velocity jet from the radial leg to the toroidal one. This high-velocity jet now is responsible for higher inertial sensitivity of the flow. Figure 5.19 shows further that for all inclinations the dependence $\Delta p \sim N^{-1/3}$ remains unchanged.

Results obtained theoretically by AM have been obtained for the inclined bend flow by Moon & Walker (1990) or by Moon, Hua & Walker (1991). Here we compare the results obtained by the approach of Bühler (1994) with the experimental data. The agreement between the measured and calculated values of potential for both cases $\Theta_z = -5^\circ$ and $\Theta_z = 15^\circ$ as shown in figures 5.20 and 5.21 is good. The strongest discrepancy which occurs in the toroidal leg (figure 5.20P,J) can be explained by the inhomogeneity of the available experimental magnetic field.

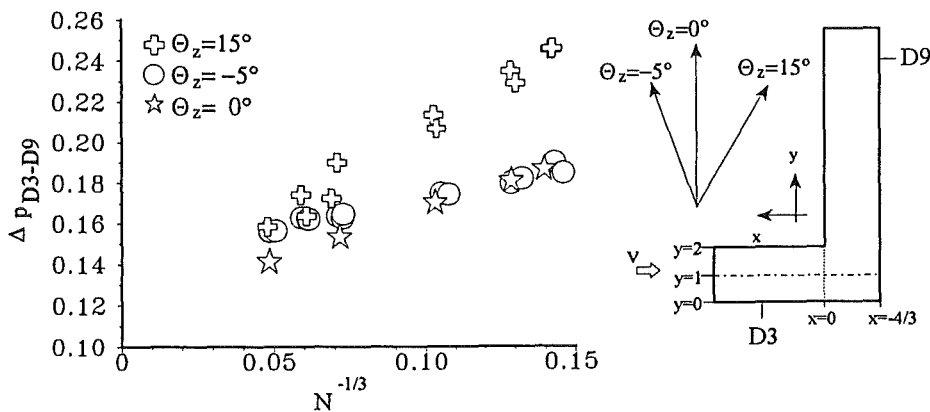


Figure 5.19 Total pressure drop for different values of the inclination angles $\Theta_z = -5^\circ, 0^\circ, 15^\circ$ as a function of the interaction parameter N at a Hartmann number $M=4175$. (Stieglitz 1994).

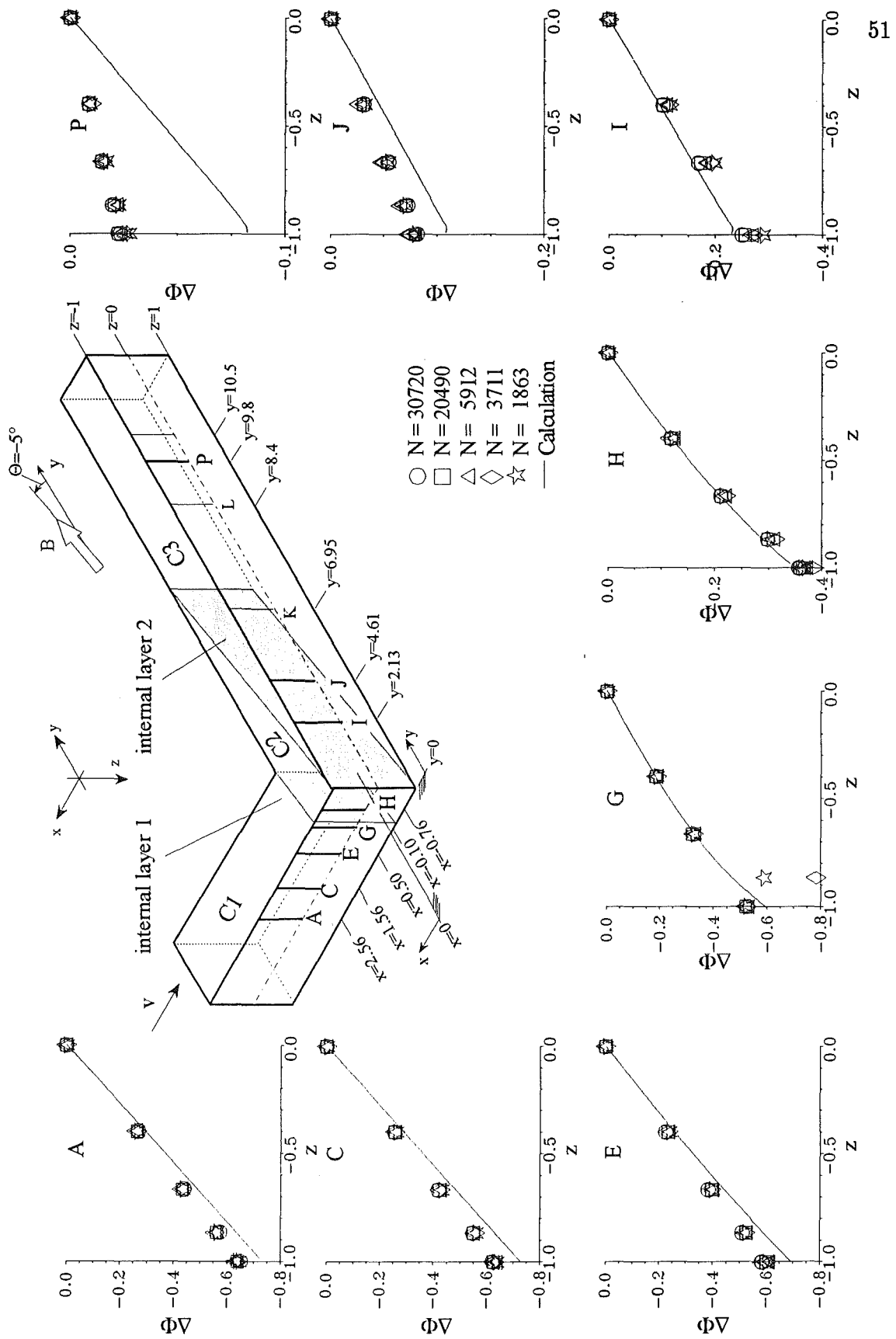


Figure 5.20 Wall potentials for an inclination angle $\Theta_z = -5^\circ$ at the positions A–P for different values of the interaction parameter N at a Hartmann number $M = 8125$, compared to the asymptotic theory $N, M \rightarrow \infty$. (Stieglitz 1994).

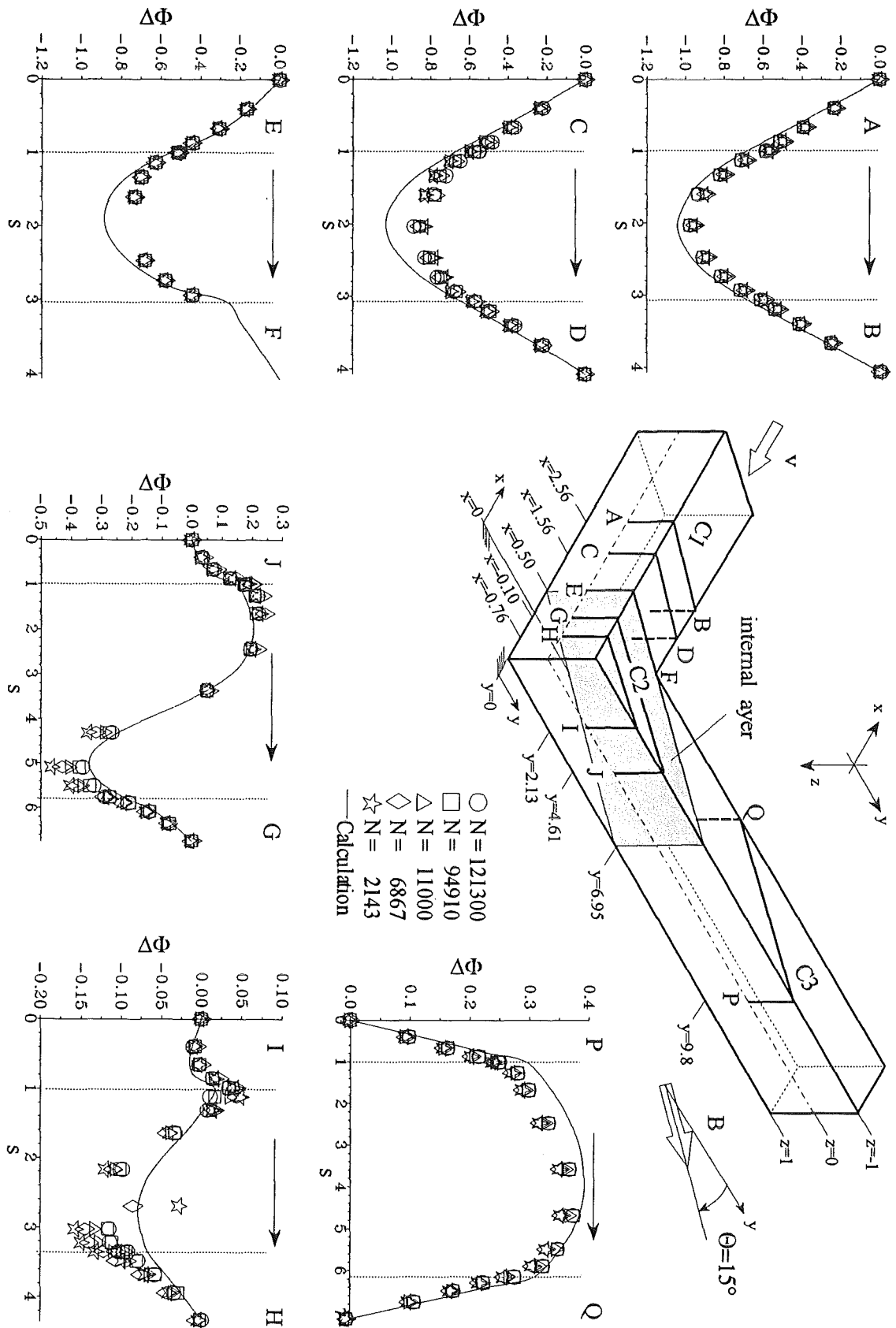


Figure 5.21 Wall potentials for an inclination angle $\Theta_z = 15^\circ$ at the positions A-P for different values of the interaction parameter N at a Hartmann number $M = 8125$, compared to the asymptotic theory $N, M \rightarrow \infty$. (Stiegholz 1994).

5.4 Multi-channel flows

Any blanket design consists of an arrangement of a number of parallel channels. In the case when these channels are electrically insulating the flow in each sub-channel may be considered as the completely decoupled single channel flow as discussed before. If there is no insulation at a common conducting wall separating the fluids of two adjacent ducts then generally, there is an electrical coupling between the ducts, which we furtheron call the *multi channel flow* (MCF).

MCFs have been considered e.g. by McCarthy & Abdou (1991) for an array of three channels as shown in figure 5.22a. In this arrangement the potentials along the side wall have almost the same values at the junction of two ducts if the flow rates in the sub-channels are the same. Therefore no significant effects in MCFs are observed. Only for strongly different flow rates in the sub-channels or for different wall conductance ratios an influence due to MCFs is observed.

With respect to applications in the radial-toroidal blanket concept (Malang *et al.* 1988) the arrangement of channels as shown in figure 5.22b is more interesting as it represents the radial duct configuration. Here the potentials at dividing conducting walls can sum up along the whole array of sub-channels. The current can cross the walls and pass via all sub-channels, thus causing a strong electromagnetic coupling. Especially this case is investigated by the following considerations in more detail.

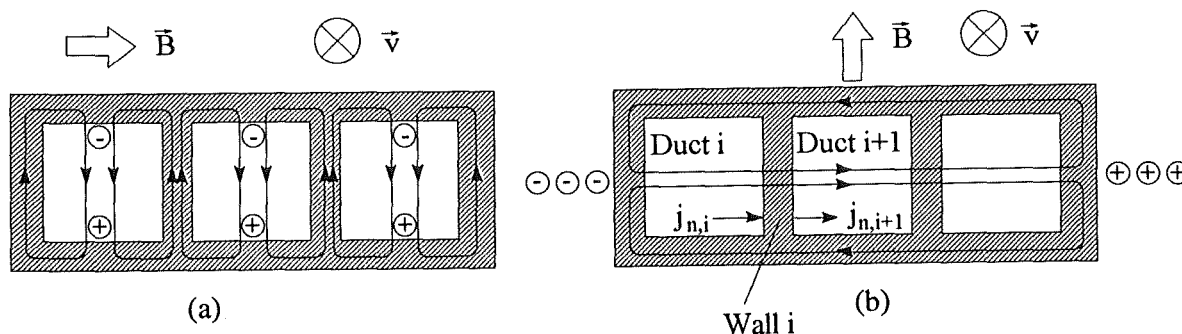


Figure 5.22 Multi channel duct flow for two possible orientations of the magnetic field.

5.4.1 Straight duct flow

The MHD flow in an array of sub-channels as shown in figure 5.22b with conducting dividing walls has been analyzed by Molokov (1993^{a,b}). In his calculations he used the flow variables v, b which correspond to the fluid velocity and to the induced magnetic field or the stream function for current, respectively. Since this approach leads to results only for fully developed flow conditions we do not refer to this formulation in more detail. To keep the notation introduced before using v, ϕ , the velocity and the potential, Molokov's basic ideas are expressed using these quantities, which can also serve for calculations in more complex 3D geometries.

The flow in each sub channel is described by the asymptotic formulation (3.4-3.9). The walls are assumed to be thin and to have perfect contact with the liquid metal so that the thin-wall condition (2.9) can be directly applied at all the outer walls. At conducting dividing walls this condition needs some modification. Since only a part of the current j_i which enters the wall i from the duct i at one side turns in the tangential direction and produces there a distribution of wall potential $\phi_{w,i}$. The rest of the current entering the wall at one side may leave it at the other side towards the adjacent sub-channel $i+1$ (see figure 5,22b).

$$j_{n,i} - j_{n,i+1} = c_i \Delta_t \phi_{w,i} . \quad (5.6)$$

This coupling condition allows the global current path across all sub-channels.

Equation (5.6) shows immediately some interesting features. If the pressure gradient $\nabla p = j \times B$ (in the asymptotic limit $M, N \rightarrow \infty$) is constant in each sub-channel the currents entering and leaving the side walls have to be equal $j_{n,i} = j_{n,i+1}$. There is no net current flux into the wall so that the potential $\phi_{w,i}$ becomes the same linear function between the two Hartmann walls as for the core potentials $\phi_{C,i}$. Flow rates $Q_{i,R,L}$ of $O(1)$ carried by high-velocity jets along the right and the left side of the wall i occur only if there exists potential differences between the cores and the walls. For the same pressure gradients in each channel they do exist only at the outer sides but they do not exist along the dividing walls. Thus the MCF in this case is comparable to a single channel flow in a duct with a width of the whole multi channel array.

More interesting is the case when instead of the pressure gradients the flow rates are equal in all the sub-channels. This case is even more desirable because it ensures a homogeneous convective heat removal by the array of channels. Equal flow rates result not necessarily in equal pressure gradients and thus cause different currents at both sides

of the dividing walls. Equation (5.6) leads for this case to a parabolic variation of potential ϕ_w along the dividing wall. Since the potential differences across the right and left side layer at the dividing wall, $\phi_{w,i} - \phi_{C,i}$, $\phi_{C,i+1} - \phi_{w,i}$, respectively, are the same but with opposite sign (since $\phi_{C,i} = \phi_{C,i+1}$) the high-velocity jets in the layers have different directions. In one duct the flow rate carried by the layer contributes to the total flow rate while in the adjacent duct it acts in opposite direction.

If the wall conductance ratios of the sub-channels vary in addition to the pressure gradient the velocity profiles may become even more peculiar. Results for different numbers of sub-channels and for different wall conductance ratios are shown in figure 5.23.

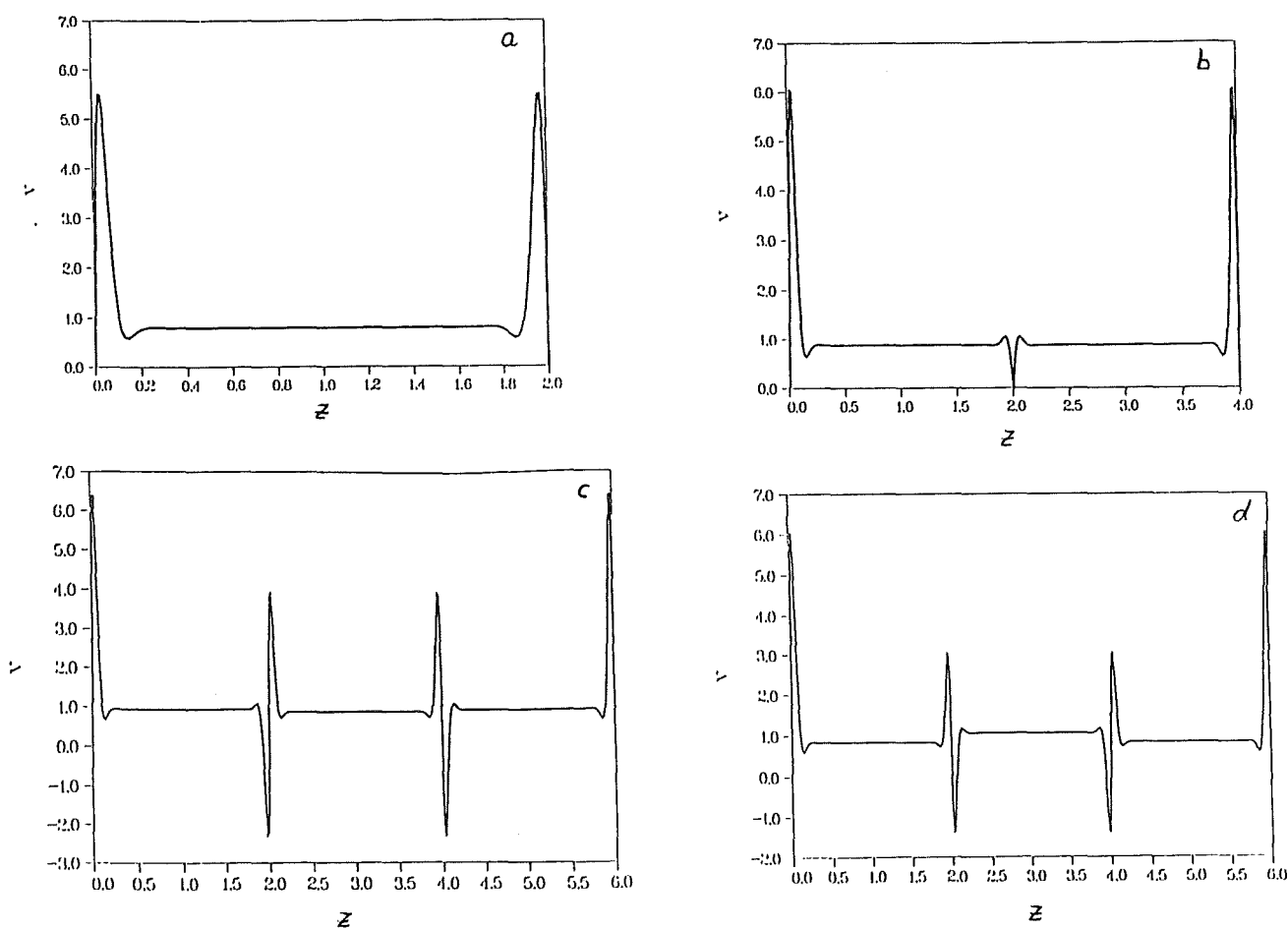


Figure 5.23 MHD flow for different numbers of square sub-channels (Molokov 1993). Velocity profiles at $y=0$ for $M=1000$ and

- a) Single duct ($n=1$), $c_H=c_S=0.1$
- b) Two ducts ($n=2$), $c_H=c_S=0.1$ for all i
- c) Three ducts ($n=3$), $c_{H1}=c_{H3}=c_{S1}=0.1$, for all i , $c_{H2}=0.2$
- d) Three ducts ($n=3$), $c_H=c_S=0.2$ for all i .

5.4.3 Multi-bend flow

In the blanket concept proposed by Malang *et al.* (1988) a large number of parallel toroidal ducts is fed by the radial ones. At the opposite toroidal end of the blanket segment the flow direction turns again to the radial direction. Thus, the front part of the blanket is formed by an array of radial-toroidal-radial U-bends. As explained already in the previous paragraph conducting dividing walls lead to an overall current path and a summation of potentials induced in the radial sub-channels where the flow direction is perpendicular to the applied strong magnetic field. Here only the most important results of this work are summarized. The high resulting voltage may cause now extreme 3D effects leading to high pressure drop near the radial-toroidal junction. There exists in addition the possibility of a current short-cut between one radial leg and the other one via the toroidal ducts. Such a current path becomes possible since the high voltages in both radial legs are induced with opposite sign. That this may lead to severe design problems has been realized already years ago (Madarame 1984).

In order to investigate the MHD flow in a number of parallel U-bends a test section of five sub-channels as shown in figure 5.24 has been used. A more detailed description of the test section as well as of all obtained experimental results is given by Stieglitz 1994. The channels are numbered starting from the inner one which contains the plane of symmetry $z=0$. The weak inclination of the entrance part by the small angle of $\Theta_z=7^\circ$ was needed to study the sensitivity with respect to small inclinations of the whole test section in the available test volume of the laboratory magnet. The part of the test section in which the flow is analyzed with prior interest is the upper half with $x < 10$ (see figure 5.24).

In order to investigate the influence of the number of sub-channels, the channels 1, 2, 3 are filled subsequently. Nevertheless, the empty channels 2 and 3 or 3 may have an influence on the flow in the filled channels due to their electrically conducting walls. This fact has been taken into account in an accompanying analysis, where the currents in all duct walls are modeled including the walls of empty channels. The experiments have been performed with both operation modes, equal flow rates $q_i = \text{const}$ or equal pressure drops $\Delta p_i = \text{const}$ in the sub-channels. Here only the first mode is discussed in detail because of its relevance concerning homogeneous convective heat removal. For the case of constant pressure drop the overall results are similar and the pressure drops are a little smaller.

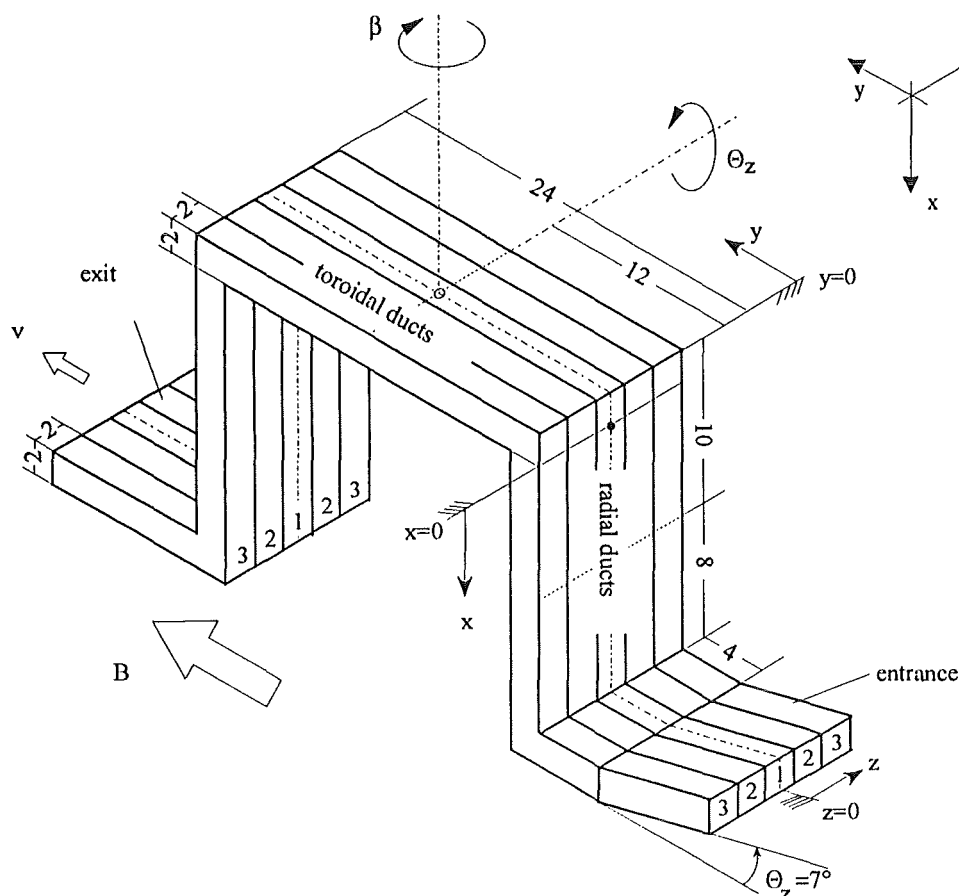
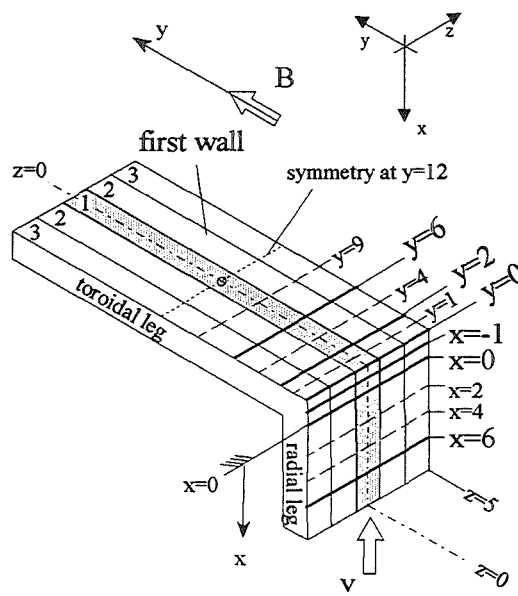
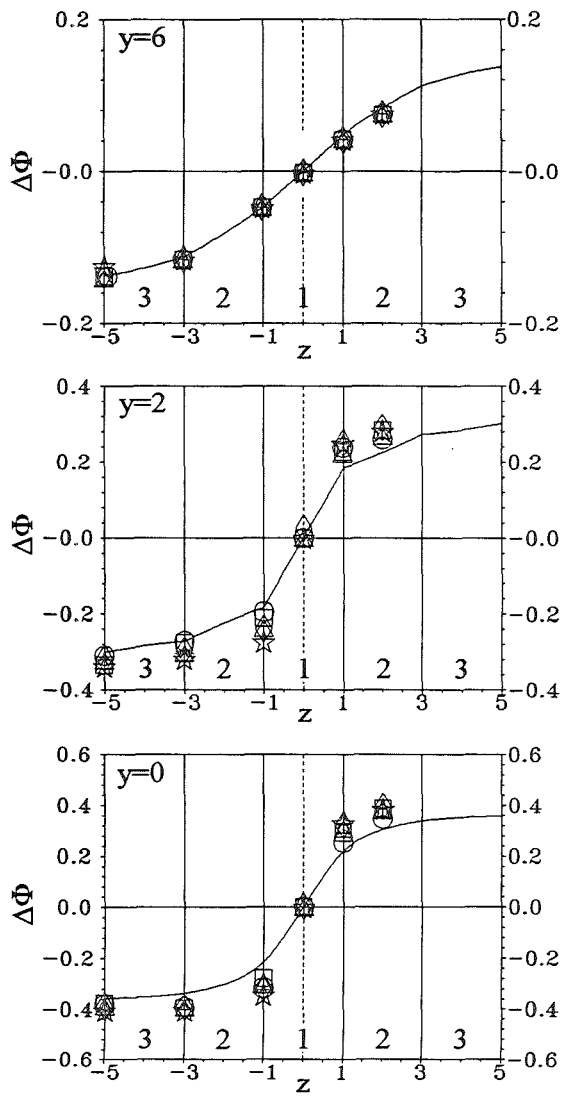


Figure 5.24 Multi-bend test section. Geometry and coordinates (Stieglitz 1994).

I. Wall potentials: For a comparison of analytically obtained results by AMs with the experimental data also the potential values at the walls of empty channels are shown (see e.g. figure 5.25–5.27).

Figure 5.25 shows the wall potential for the single bend flow (1BF) where only the inner bend $i=1$ is filled with liquid metal. The almost perfect agreement between measured and calculated data for the potential confirms further that good symmetry conditions have been achieved experimentally. Further on, only the part $z > 0$ is shown for the 3-bend flow (3BF) for different values of M (figure 5.26), for different values of N (figure 5.27), and for 5-bend flows (5BF) (figure 5.28). In all cases considered the agreement between theoretically and experimentally obtained potentials is surprisingly good even if the used asymptotic theory does not account for inertia or for viscosity. Only near the radial toroidal junction at the positions $x \leq 0$ for 3BF or at the positions $x \leq 0$, $y \leq 2$ for 5BF larger differences are measured. The range of positions where the disagreements occur is small and indicated by the hatched surface of the geometry in figure 5.28. Although the strongest inertia effect are expected in this part of the bend the discrepancy between theory and experiment does not disappear even for the highest investigated values of N so that it can not be explained by inertia forces only.



- $N=32390$
- $N=23900$
- △ $N=9436$
- ◇ $N=5778$
- ☆ $N=2004$
- + $N=1101$
- Calculation

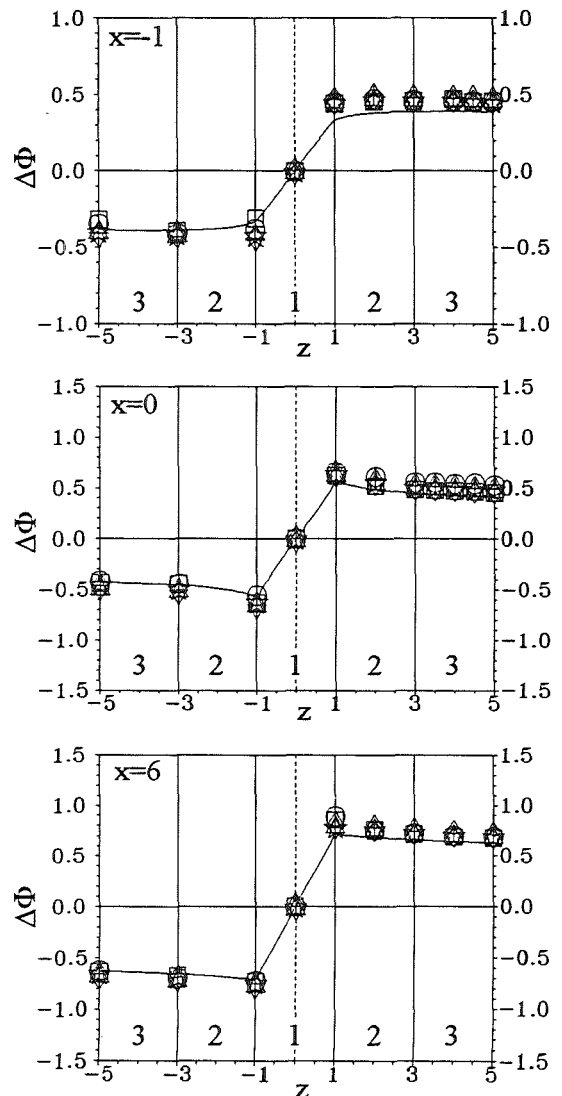


Figure 5.25 MHD flow in the center bend $i=1$, bends $i=2,3$ are empty. Wall potentials at different positions as indicated in the sketch of geometry. $M=2365$, $c=0.038$, $\theta_z=0$. (Stieglitz 1994).

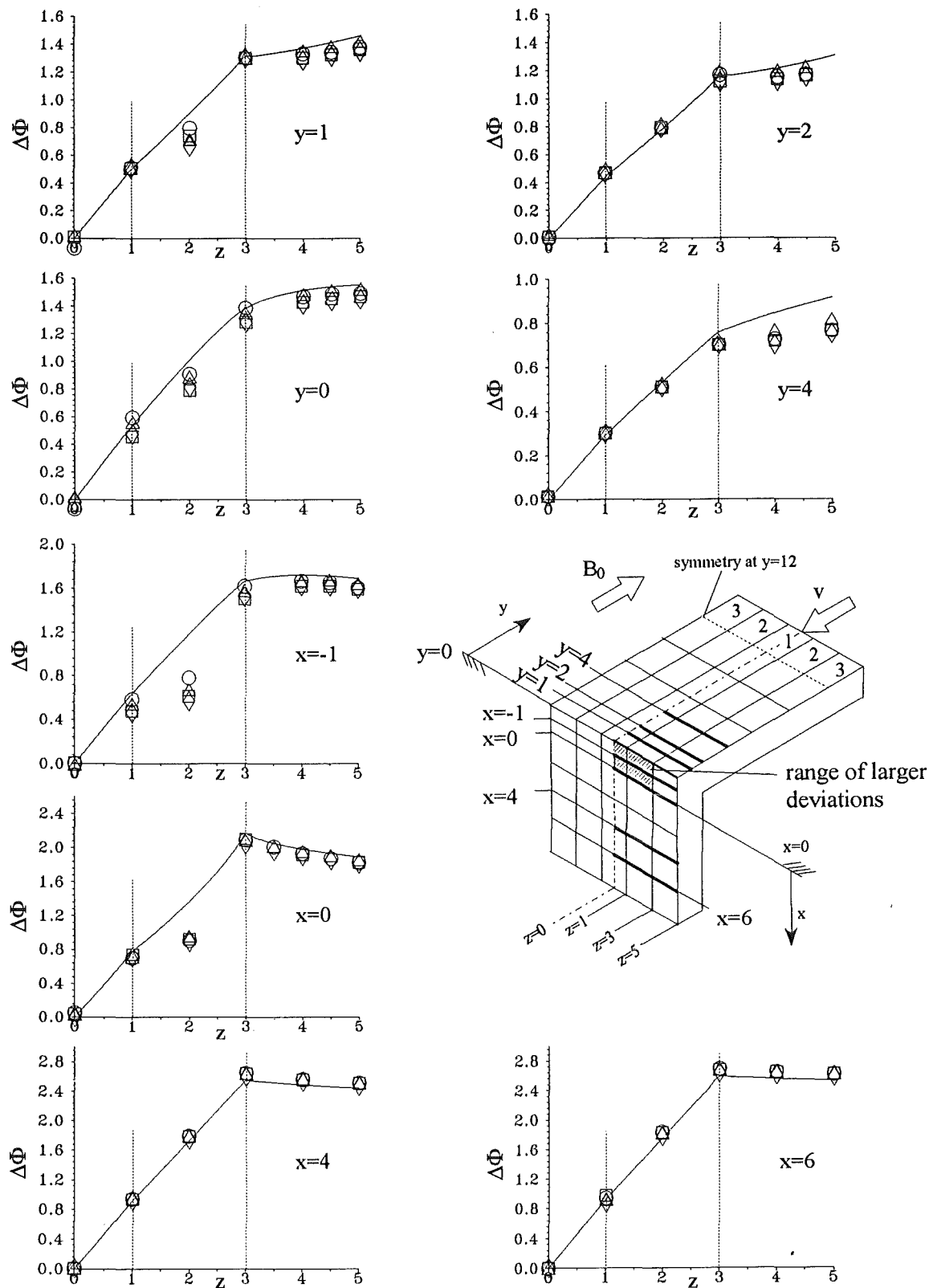


Figure 5.26

MHD flow in the inner bends $i=1,2$, bends $i=3$ are empty. Wall potentials at different positions as indicated in the sketch of geometry. $N=1034$, $c=0.038$, $\Theta_z=0$. $M=2431$ (\circ), 1910 (\square), 1211 (\triangle), 634 (\diamond), calculation (—). (Stieglitz 1994).

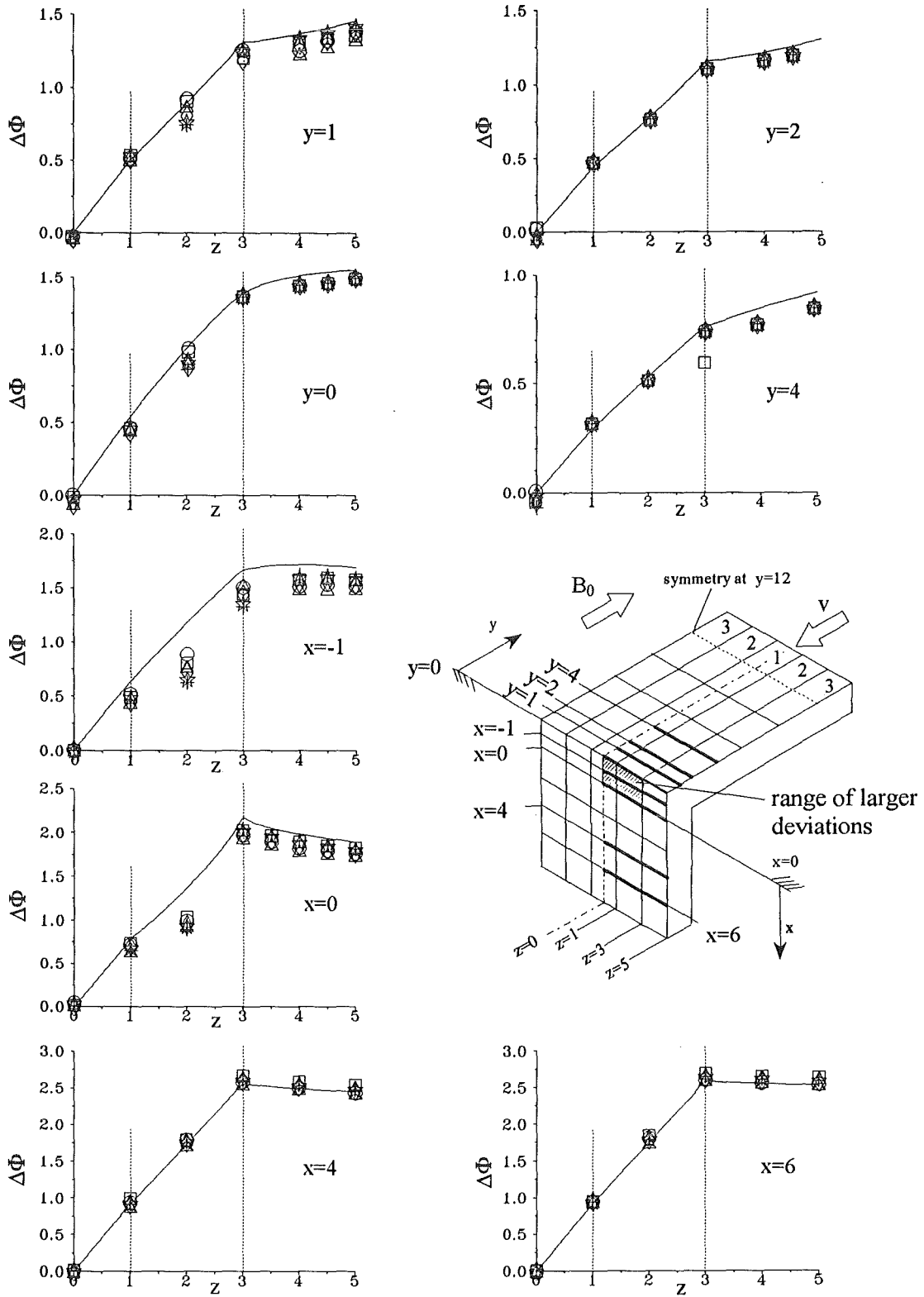


Figure 5.27 MHD flow in inner bends $i=1,2$, bends $i=3$ are empty. Wall potentials at different positions as indicated in the sketch of geometry. $M=2431$, $c=0.038$, $\Theta_2=0$. $N=37436$ (\circ), 20355 (\square), 10457 (Δ), 4153 (\diamond), 1827 ($*$), 1034 ($+$), calculation (—) (Stieglitz 1994).

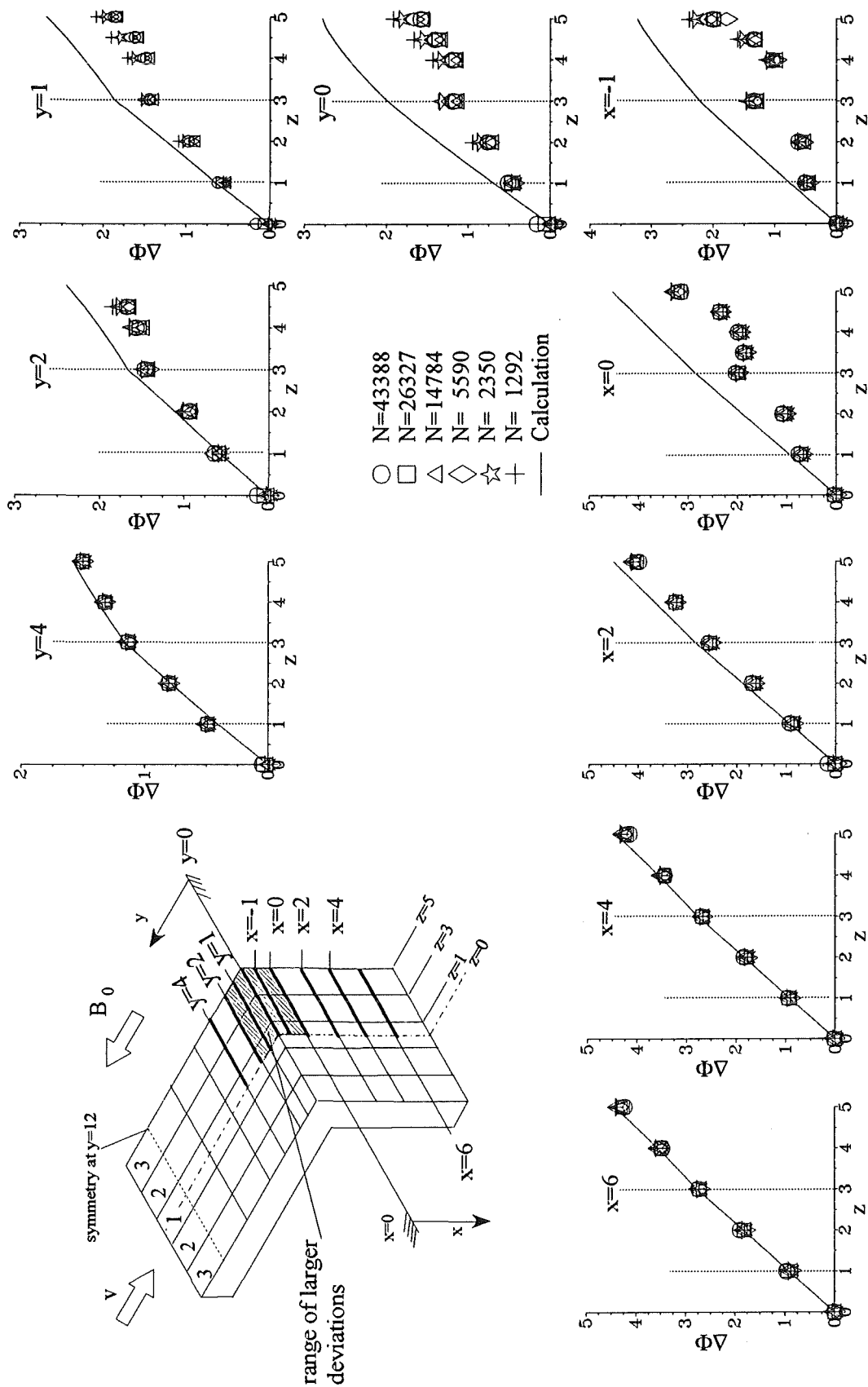


Figure 5.28

MHD flow in all bends $i=1,2,3$. Wall potentials at different positions as indicated in the sketch of geometry. $M=2372$, $c=0.038$, $\Theta_z=0$. $N=43388$ (○), 26327 (□), 14784 (△), 5590 (◇), 2350 (*), 1292 (+), calculation (—). (Stieglitz 1994).

II. Pressures: Measurements of the pressure differences between the positions (i,k) have been performed for a number of different cases. Here the first index i denotes the channel number, the second one k stands for the position along the U-bend. Figure 5.29 shows the pressure drop in the center of the duct $i=1$ between the positions $k=1$ and $k=2$. A comparison of the experimental data with the AM results for fully developed 2D flows shows good agreement for the single bend flow (figure 5.29b) indicating that the radial part used in the experiment has been long enough to provide fully developed conditions between the positions 1.1 and 1.2. In the case of a 3BF the results of fully developed 2D pressure drop and the measured pressure data do not agree, even for the highest value of N , indicating that the radial length is too short for the flow to become fully developed. This can be confirmed by detailed 3D calculations including the entrance part of the geometry and, in addition, the wall conductivity of the empty channels. If all these effects are taken into account the AM predicts the experimental findings almost exactly for high values of N . The same tendency is observed for the 5BF. A comparison of all measured radial pressure differences show that the pressure differences 1.1–1.2 increases with the number of filled channels. Inertialess conditions are already reached for the 1BF at moderate N of 10^3 . In the 3BF inertialess flow is reached at $N \geq 10^4$, while for 5BF it has been not yet reached even at the highest investigated value of N . In all cases considered the inertia effects increase the pressure drop.

In figure 5.30 the pressure drop along the whole U-bend between the positions $i.2-i.5$ is shown as a function of the interaction parameter. The pressure drops are shown versus the $N^{-1/3}$ -axis to demonstrate the dependence $\Delta p_{3D} \sim N^{-1/3}$ by the linear behavior of the experimental data for all cases considered (1BF, 3BF, 5BF). The agreement in the inertialess limit as $N^{-1/3} \rightarrow 0$ with the results obtained by inertialess AM is good for 1BF and also for 3BF. In case of the 5BF the pressure drop in the outer channels is comparable to the predicted values. The inner channels 1 and 2 show differences of about 30% in comparison to the theoretically obtained pressure data. Although the dependence of $\Delta p_{3D} \sim N^{-1/3}$ is confirmed for different numbers of bends (1,2,3) the influence of inertia effects is more pronounced for higher channel numbers. It can reach two times (3BF) or three times (5BF) the value of inertialess flow.

At smaller values of N i.e. $N^{-1/3} > 0.25$ the pressure drop correlation $\Delta p_{3D} \sim N^{-1/3}$ is changed to a weaker dependence due to turbulent effects.

In all cases considered the highest pressure drop has been observed in the inner channel $i=1$. It decreases continuously with higher N , but increases with the number of filled channel linearly up to the number of five bends considered (see figure 5.31).

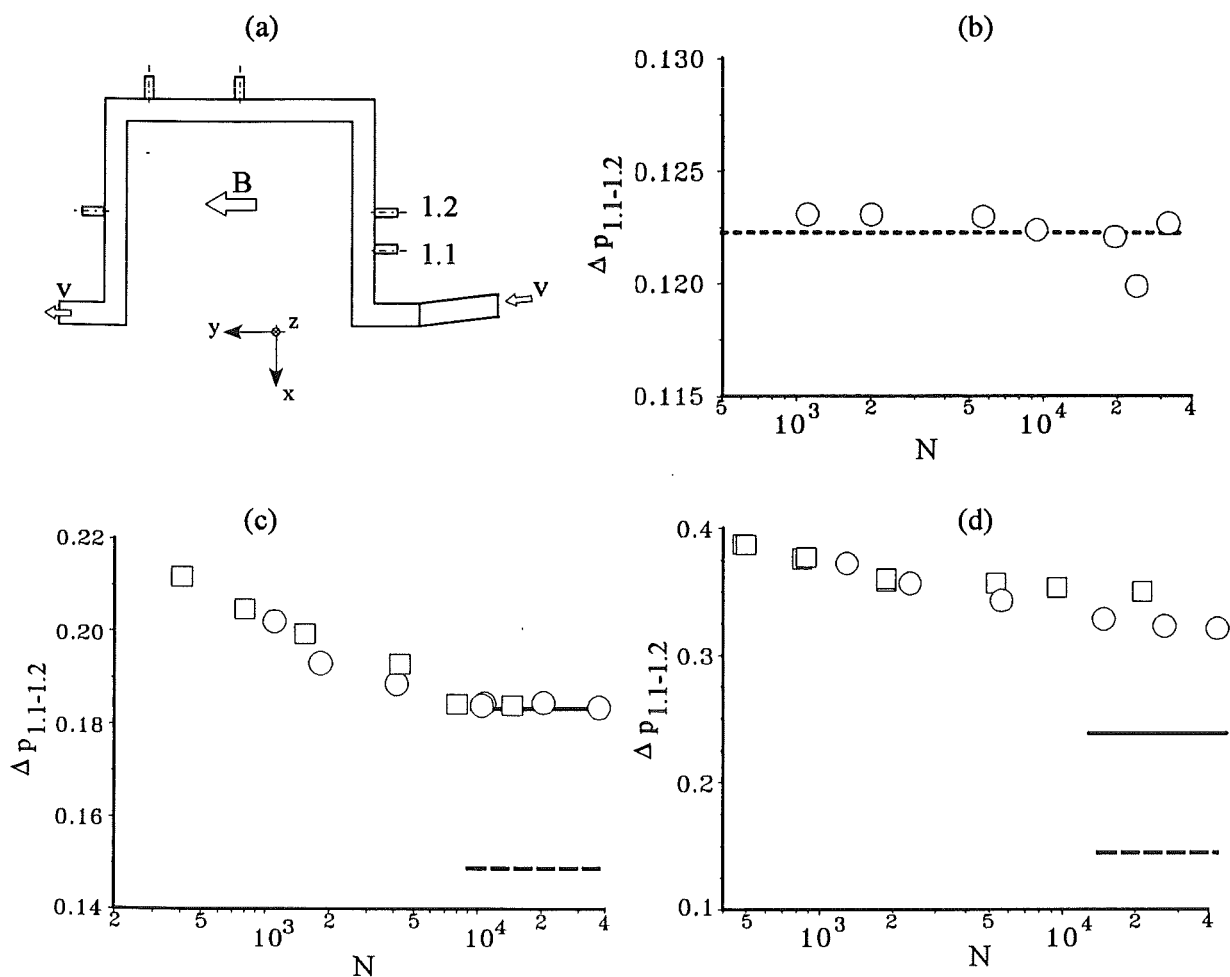


Figure 5.29 Pressure drops in the radial part of multi-bend flows as a function of the interaction parameter N . $c=0.038$, $\Theta_z=0$. a) Sketch of geometry, b) 1BF, c) 3BF, d) 5BF, for $M=1800$ (\square), 2400 (\circ). 2D calculations with $M=2400$ (---), 3D calculations taking into account all conducting walls (—). (Stieglitz 1994).

II. Sensitivity to small inclinations: Small inclinations of the toroidal duct with respect to the magnetic field do lead to some small increase in pressure drop. Compared to the total pressure drop this value is insignificant for all cases considered (see Stieglitz 1994) and is therefore not discussed here in more detail.

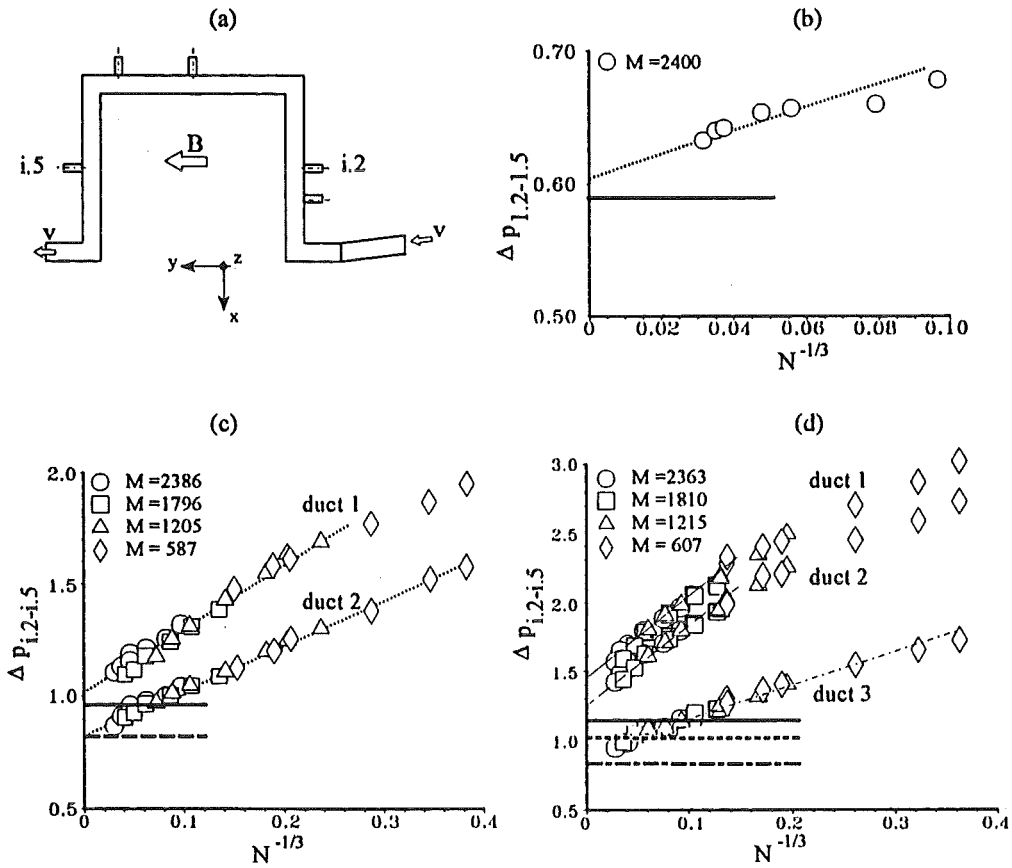


Figure 5.30 Total pressure drops in multi-bend flows as a function of the interaction parameter N . $c=0.038$, $\Theta_z=0$. a) Sketch of geometry, b) 1BF, c) 3BF, d) 5BF. 3D calculations bend 1 (—), bend 2 (---), bend 3 (-·-·-). (Stieglitz 1994).

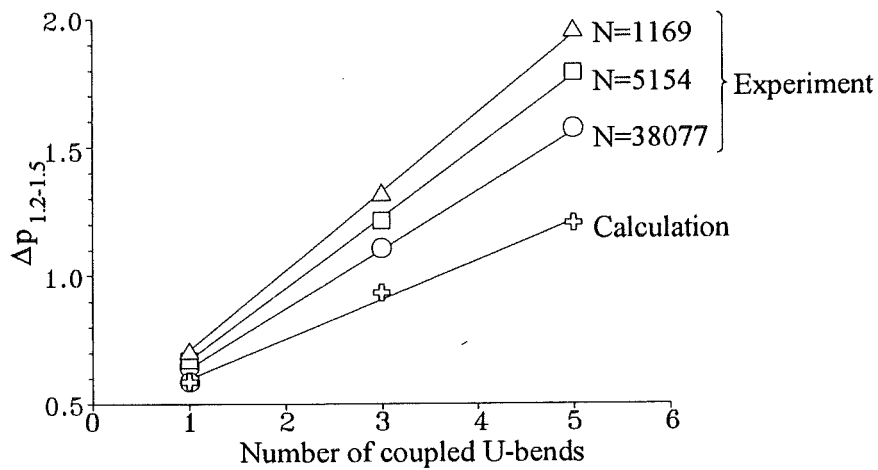


Figure 5.31 Total pressure in the bend $i=1$ for different interaction parameters as a function of the number of filled channels. $M=2402$, $c=0.038$, $\Theta_z=0$. (Stieglitz 1994).

5.4.3 Pressure drop reduction in multi-bend flows

A significant reduction of the pressure drop in multi-bend flows can be achieved by an electrical separation of the ducts. Direct insulating coatings at all walls would eliminate MCF completely. In the following chapters it is investigated whether such strong insulating conditions are necessary or if it is possible to get a reduction even by simpler means.

To analyze this problem only the radial part of the bend has been electrically separated at the side walls as shown in figure 5.32. The dividing radial side walls are split into two conducting sheets separated electrically by a thin layer of insulating material. The ducts are still connected via the conducting Hartmann walls. Such a simple configuration allows a reduction of total pressure drop over the whole range of the interaction parameter of about 30% for the 3BF and even more for 5BF (see figure 5.33). Nevertheless it does not completely avoid 3D effects caused by multi-bend flows. Only if the radial ducts are completely decoupled (e.g. by means of direct insulating coatings or by FCIs, the toroidal ducts are still coupled) that additional pressure drop due to an electrical coupling between the channels does not exist. In this case the pressure drop of multi-bend flow is the same in each bend and only little higher than in the single bend flow (Reimann *et al.* 1993).

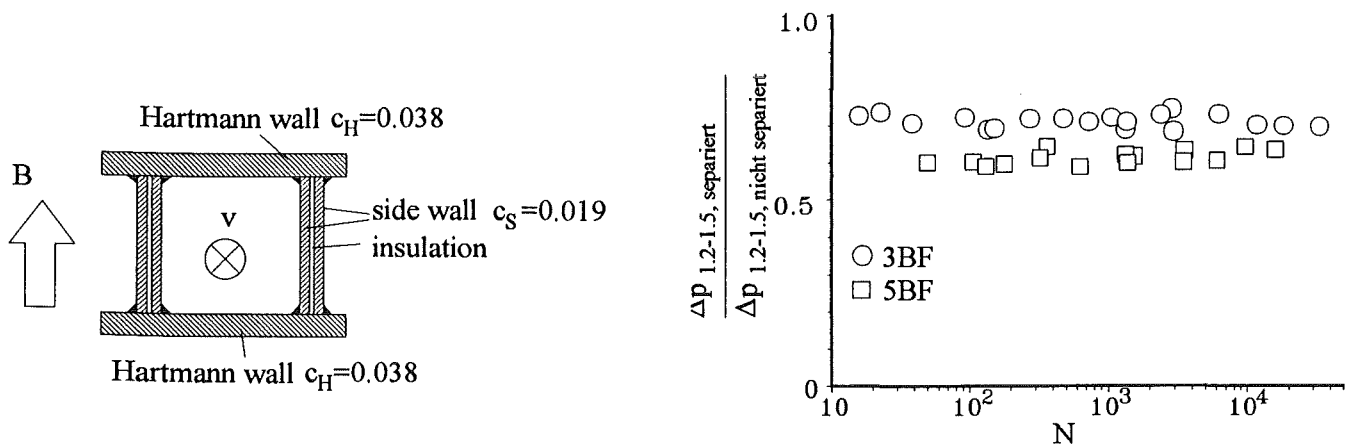


Figure 5.32 a) Electrically separated dividing side walls of radial ducts. b) Pressure drop reduction in multi-bend flows. 3BF (\circ), 5BF (\square). (Stieglitz 1994).

5.4.3 Manifolds

Necessary elements to achieve multi channel flows are manifolds which distribute the fluid from larger supplying ducts to several sub-channels. This may cause MHD effects if the distribution happens in the region of the magnetic field. The first detailed investigations for the pressure drop in a manifold with conducting walls from which the upper half is shown in figure 5.33 have been performed by Hua & Picologlou (1991). They find only marginal values of additional pressure drop due to the flow distribution to sub-channels so that they conclude:

" The results of the examples presented here indicate that pressure drop associated with manifolds of the type discussed here is only a small fraction of the overall pressure drop, and that desirable flow distribution among coolant ducts can be achieved with a judicious choice of wall thickness distribution. As a result the MHD effects related to manifolds of this type can be neglected during the blanket conceptual design phase."

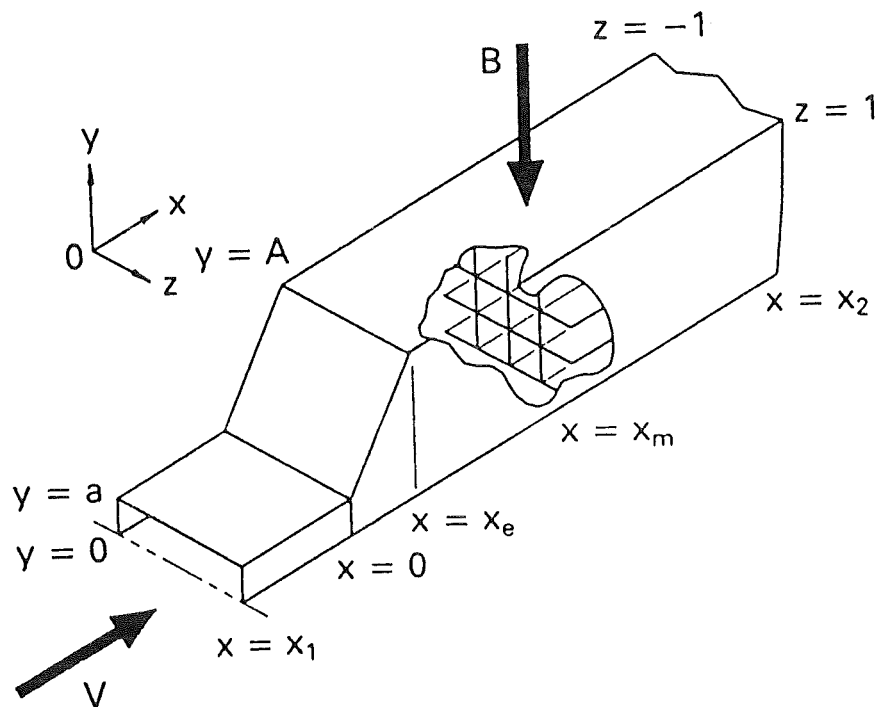


Figure 5.33 Geometry of a conducting manifold (Hua & Picologlou 1991).

For the case of insulating duct walls Molokov (1994) presents solutions for manifolds with expansions or bends in the plane perpendicular to the field. He also finds negligible pressure drop due to the distribution of flow among the sub-channels for the cases considered. The velocity profiles exhibit constant core velocities along magnetic field lines. Disturbances from the slug profile in the transverse direction disappear roughly at distances equivalent to the duct width. Some examples are shown in figure 5.34.

A special type of a manifold is a T-junction. If all changes of geometry happen in the plane perpendicular to the field the MHD flow does not cause significant additional 3D effects due to the flow distribution or recombination. This can be confirmed for conducting walls (theoretically Bühler (1994), experimentally Reimann *et al.* (1994)) as well as for insulating walls (Molokov 1994).

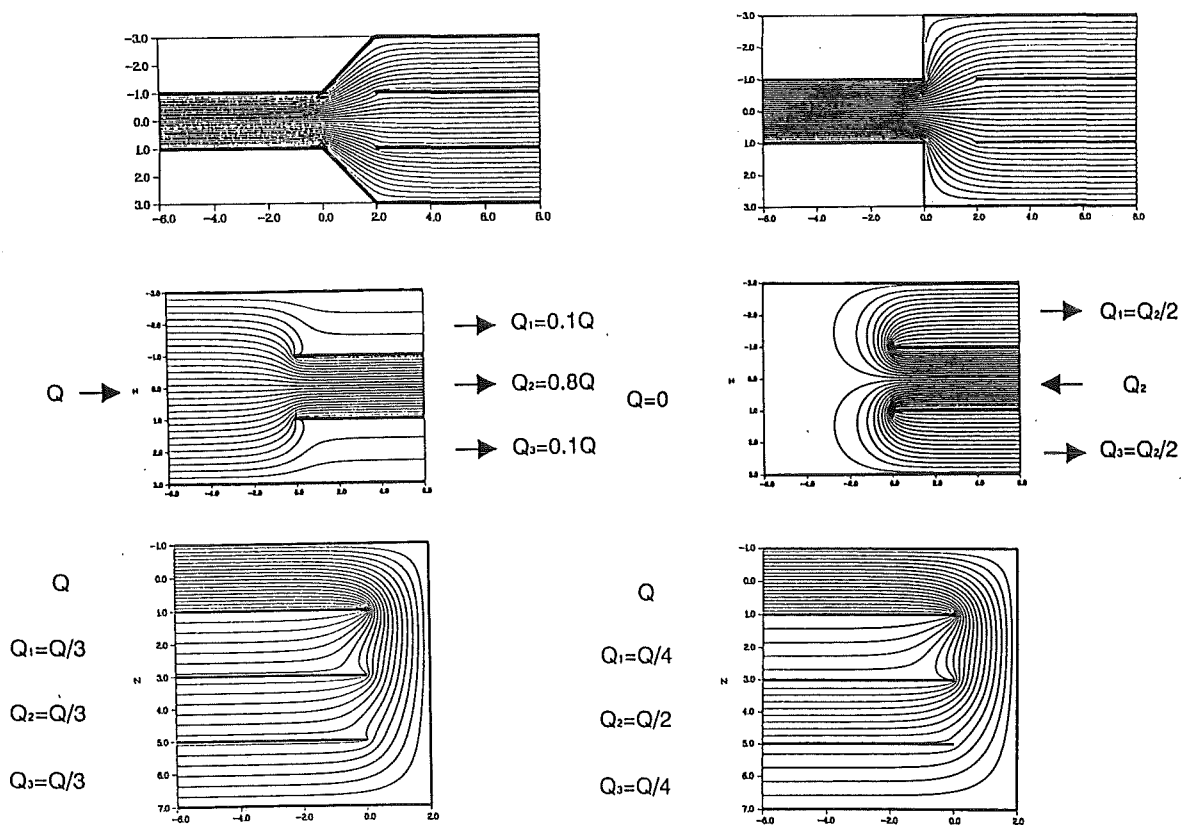


Figure 5.34 Streamlines in the plane perpendicular to the field for some manifolds (Molokov 1994).

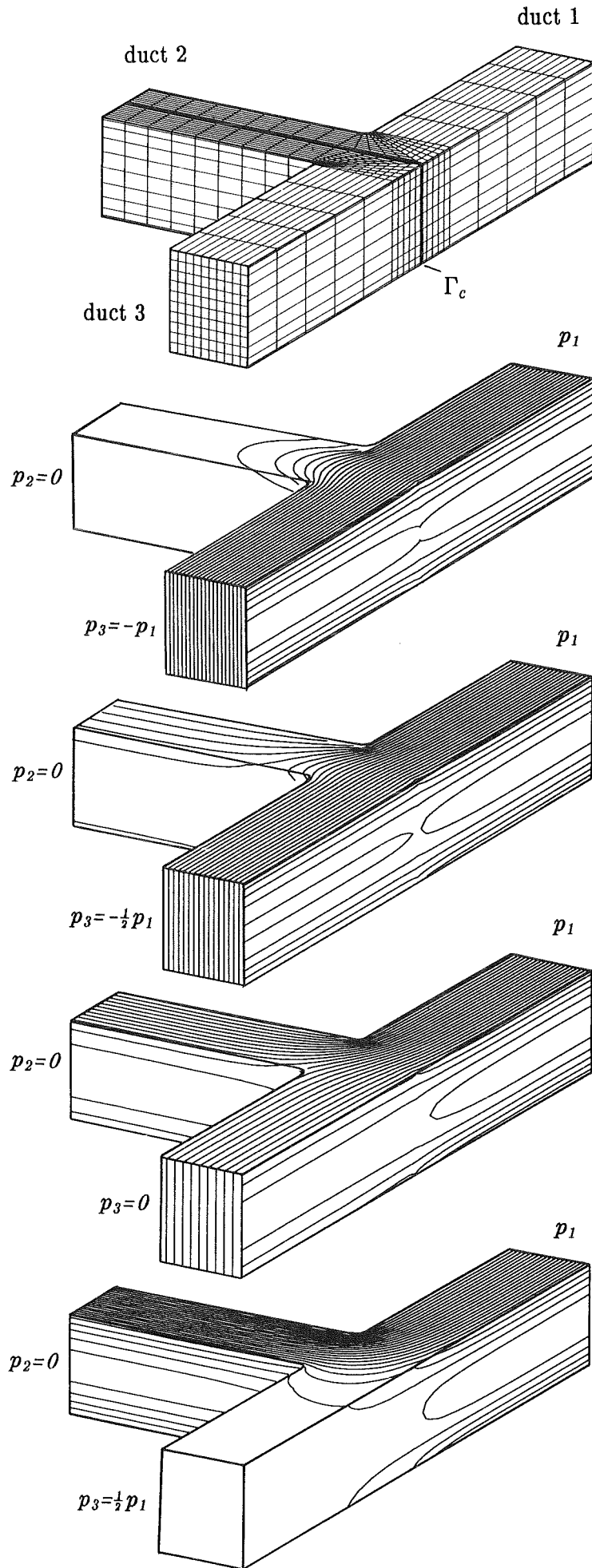


Figure 5.35 MHD flow in a conducting T-junction (Bühler 1994).

6 Conclusions

In all designs of liquid metal blankets for fusion reactors MHD flows play an important role. Flows in basic elements of blankets especially in straight ducts have been analyzed very early and are quite well understood for a long time. These old results predict high unacceptable pressure drop if the duct walls are thick and therefore highly electrically conducting. It has been shown that the pressure drop associated with the flow of the electrically conducting fluid in the strong plasma confining magnetic field can be essentially reduced by orders of magnitude if a kind of insulation is provided at the duct wall. The use of directly insulating coatings at all walls would lead to the optimum improvement concerning pressure drop. Since the technological feasibility of such coatings has not yet been demonstrated FCIs are considered as a feasible option for the near future. They do not ensure a pressure drop reduction as high as the insulating coatings but they can provide a pressure drop reduction up to 95% for straight duct flows.

Laminar 3D effects in laminar straight duct flows in the fringing magnetic field as well as in ducts of non-uniform cross section can be analyzed by AM. The results depend on the gradient of the magnetic field, on the expansion ratio and the conductivity of the channel walls. Therefore it is impossible to give global quantitative results for all possible applications. However, AM are able to predict accurately the pressure drop and the flow pattern in almost any desired 3D application in the inertialess limit. Qualitatively all results show the same tendency. The equivalent length l_{3D} characterizing the additional pressure drop compared to the flow in a straight duct of the same conductivity is larger for smaller wall conductance ratios c . For the expansion considered the maximum value of l_{3D} is reached at $c=0$. For the case of rectangular variable area cross section the highest value l_{3D} is obtained for the expansion ($2a \times 2b \rightarrow 4a \times 2b$), while for the expansion ($2a \times 2b \rightarrow 2a \times 4b$) no significant additional pressure drop is observed. This leads to the general guide line for the designers of liquid metal fusion blankets to place the expansions or contractions only in the plane perpendicular to the magnetic field in order to avoid strong additional 3D effects.

The same holds for bend flows. If the bend turns the flow only in the plane perpendicular to the magnetic field the influence on pressure drop is negligible, even if the velocity profiles are strongly affected. However, if the flow direction changes in the plane of the field significant contributions to the pressure drop associated with an intense velocity redistribution occur. These effects are most pronounced if the flow turns from a

direction originally perpendicular to the magnetic field in a direction perfectly aligned with the field like in the toroidal duct of a radial-toroidal-radial U-bend. For this case AM predict the flow rate to be confined to thin layers along all field-aligned walls. The toroidal core which does not contribute to the total flow rate is involved in an intense mass exchange between all the layers. These unexpected results have been checked by a comparison with experimental data of wall potential and pressure. The comparison shows good agreement with the potential measurements for the whole range of the parameters considered. Good agreement for pressure drop is reached for high values of the interaction parameter N i.e. in the inertialess limit. Inertial effects at small N lead to an additional inertial contribution to the pressure drop which can be quantified by an empirical correlation $\Delta p \sim N^{-1/3}$. The effects of small inclinations of the toroidal duct with respect to the magnetic field direction is small and can be described by A.A for high values of N .

The electrical coupling between neighboring channels at joint dividing and conducting walls lead to peculiar flow pattern even in fully developed flows if the pressure gradients or the wall conductance ratios in the sub-channels are different. More pronounced and quite severe are the effects arising from the electrical coupling at joint walls of an array of radial-toroidal-radial U-bends. A comparison of experimental data and predicted values of wall potential shows good agreement in the radial and in the toroidal legs except a small region near the outer corner where some discrepancies are observed. These regions are increasing in size with the number of parallel channels. While in the case of 3BF the pressure drops predicted by AM agree almost perfectly with the inertialess limits of the experimental data in the case of 5BF the agreement is still good for the outer ducts, but deviations up to 30% occur in the center ducts. As in the single bend flow the additional inertial contributions to the pressure drop scale with $N^{-1/3}$. The total pressure drops which increase linearly with the number of investigated channels can be reduced significantly by an electrical separation at the dividing walls of the radial ducts. A pressure drop very close to the one observed in 1BF can be obtained by a total electrical decoupling of the radial channels.

All calculations and experiments show that liquid metal flows in fusion blankets can be established at acceptable pressure drop if an efficient insulation method is applied to separate the fluid from the well conducting channel walls. AM form the basis of efficient tools for calculating the pressure drop and flow pattern in the laminar inertialess limit. Empirical pressure drop correlations obtained from experimental data give the inertial corrections which scale for all cases considered with $N^{-1/3}$.

This report summarizes the present knowledge of MHD flows in basic elements of fusion blankets. Even if many problems have been solved one should keep in mind that there are still questions to be answered. The question of 3D effects in insulating rectangular ducts with one pair of walls perfectly aligned with the magnetic field is currently under investigation. The inertial part of the pressure drop has been quantified by empirical correlations on the basis of experimental data, but still a tool for its theoretical prediction is not available. For future work one should keep in mind the fact that even in strong magnetic fields the flow may lose its laminar stability and exhibit time-dependent or turbulent characteristics. The problem of heat transfer in MHD flows which has not been addressed in this report is also a challenging task and currently under investigation.

References

- Aitov, T.N., Kalyutik, A.I., Tananaev, A.V. 1979 Numerical investigations of three-dimensional MHD-flow in a curved channel of rectangular cross section. *Magnetohydrodynamics*, 4, 82–87.
- Badger, B. et al. 1974 UWMAK-I a Wisconsin toroidal reactor design. *University of Wisconsin*, report UWFDM-68.
- Barleon, L., Bühler, L., Mack, K.-J., Stieglitz, R., Picologlou, B.F., Hua, T.Q., Reed, C.B. 1992 Investigations of liquid metal flow through a right angle bend under fusion relevant conditions; Proceedings of the 17th Symposium on Fusion Technology (SOFT), Rom; *Elsevier SCIENCE Publishers B.V.*, II, 1276–1280.
- Barleon, L., Casal, V., Mack, K.-J., Kreuzinger, H., Sterl, A., Thomauske, K. 1989 Experimental and theoretical work on MHD at the Kernforschungszentrum Karlsruhe – the MEKKA-program; Liquid Metal Magnetohydrodynamics (Lielpeteris, J.; Moreau, R. editors); *Kluwer Academic Publishers*, 55–61.
- Barleon, L., Casal, V., Lenhardt, L. 1991 MHD-flow in liquid metal cooled blankets. *Fusion Engineering and Design*, 14, 401–412.
- Barleon, L., Lenhart, L., Mack, K.J., Sterl, A., Thomauske, K. 1989 Investigations on liquid metal MHD in straight ducts at high Hartmann numbers and interaction parameters. Proceedings of Fourth International Topical Meeting on Nuclear Reactor Thermal-Hydraulics NURETH-4, Karlsruhe, 2, pp. 857–862.
- Boyarevich, A.V. et al. 1990 Measurement of averaged local velocities in magnetohydrodynamic experiments. *Magnetohydrodynamics*, 26, 133.
- Bühler, L. 1991 Liquid metal flow in arbitrary thin-walled channels under a strong transverse variable magnetic field. *Fusion Engineering and Design*, 17, 215–220.
- Bühler, L. 1993 Magnetohydrodynamische Strömungen flüssiger Metalle in allgemeinen dreidimensionalen Geometrien unter der Einwirkung starker, lokal variabler Magnetfelder. *KfK report*, KfK5095.

- Bühler, L. 1993 Additional magnetohydrodynamic pressure drop at junctions of flow channel inserts. Proc. of the 17th SOFT, Rom, Sept 14–18, 1992, Vol. 2, 1301–1305.
- Bühler, L. 1994 The influence of small cracks in insulating coatings on flow structure and pressure drop in MHD channel flows. Presentation at ISFNT–3, Los Angeles.
- Bühler, L. 1994 Magnetohydrodynamic flows in arbitrary geometries in strong, non–uniform magnetic fields. A numerical code for the design of fusion reactor blankets. To be published in *Fusion Technology*.
- Bühler, L. Molokov, S. 1993 Magnetohydrodynamic flows in ducts with insulating coatings. *KfK report*, KfK5103.
- Burr, U., Bühler, L. 1994 Wärmeübertragung in dreidimensionalen, magnetohydrodynamischen Strömungen. *KfK report*, KfK5329.
- Chang, C. Lundgren, S. 1961 Duct flow in Magnetohydrodynamics. *ZAMP*, XII, 100–114
- Gold, R. 1962 Magnetohydrodynamic Pipe flow. Part 1 *J. Fluid Mech.* **13**, 505–512.
- Hua, T.Q., Picologlou, B. 1990 Magnetohydrodynamic flow in a Manifold and multiple rectangular coolant ducts of self–cooled blankets. *Fusion Technology* **19**, 102–112.
- Hua, T.Q., Walker, J. 1988 Three–dimensional flows in rectangular ducts of liquid metal–cooled blankets. *Fusion Technology* **14**, 1389–1398.
- Hua, T.Q., Walker, J. 1989 MHD flow in insulating circular ducts for fusion blankets. *Fusion Technology* **15**, 699–704.
- Hunt, J.C.R., Leibivich, S. 1967 Magnetohydrodynamic flow in channels of variable cross–section with strong transverse magnetic fields. *J. Fluid Mech.* **28**, 241–260.
- Hunt, J.C.R., Stewartson, K. 1965 Magnetohydrodynamic flow in rectangular ducts II. *J. Fluid Mech.* **23**, 563.

John, H., Malang, S., Sebening, H. (editors) 1991 DEMO-relevant test blankets for NET/ITER. *KfK report*, KfK4908.

Kim, C.N. Hadid, A.H., Abdou, M.A. 1989 Development of a computer method for the full solution of MHD flow in fusion blankets. *Fusion Engineering and Design*, **8**, 265–270.

Kulikovskii, A.G. 1968 Slow steady flows of a conducting fluid at large Hartmann numbers. *Fluid Dynamics*, **3**(1), 1–5.

Lenhart, L. 1994 MHD Strömungen in Rechteckgeometrien. Dissertation Universität Karlsruhe.

Lenhart, L., McCarthy, A.K. 1989 Comparison of the core flow solution and the full solution for MHD flow. *KfK report*, KfK4681.

Madarame, H., Taghavi, K., Tillack, M.S. 1984 Analysis of MHD-fluid flow and pressure drop. *FINESSE Interim Report*, **3**, edited by Abdou, M. UCLA-ENG-84-30, 6.9–6.109

Madarame, H., Hagiwara, T. 1989 Computer code for analyzing liquid metal MHD flow in rectangular duct under strong transverse magnetic field. *Fusion Engineering and Design*, **8**, 167–171.

Malang, S. *et al.* 1986 Liquid metal cooled blanket concept for NET, Proc. of 14th SOFT, Avignon, Sept. 1986, *Pergamon Press Oxford* 1273–1280.

Malang, S. *et al.* 1988 Self-cooled liquid metal blanket concept. *Fusion Technology* **14**, 1343.

Malang, S., Deckers, H., Fischer, U., John, H., Meyder, R., Norajitra, P., Reimann, J., Reiser, H., Rust, K. 1991 Self-cooled blanket concepts using Pb-17Li as liquid breeder and coolant. *Fusion Engineering And Design* **14**, 379–399.

Malang, S. 1991 Development of electrically insulating coatings for Pb-17Li blankets. Presented at the *Workshop on requirements, problems and comparison of fusion reactor blanket concepts*, St. Petersburg, Oct. 17–18, 1991.

Malang, S. *et al.* 1991 Status report: KfK contribution to the development of DEMO-relevant test blankets for NET/ITER, Part 1, Self-cooled liquid metal breeder blanket. Volume 1 *KfK report*, KfK4907.

Malang, S. *et al.* 1993 Dual coolant liquid metal breeder concept. Proc. of 17th SOFT, Rom, 14–18 Sept. 1992.

Malang, S. *et al.* 1993 MHD work on self-cooled liquid-metal blankets under development at the Nuclear Research Centre, Karlsruhe. *Perspectives in Energy*, 303–312

McCarthy, K.A. 1989, Analysis of liquid metal flow using a core flow approximation with applications to calculating the pressure drop in basic geometric elements of fusion reactor blankets. Dissertation, University of California, Los Angeles.

McCarthy, K.A. Abdou, M.A. 1991, Analysis of liquid metal MHD flow in multiple adjacent ducts using an iterative method to solve core flow equations. *Fusion Engineering And Design* 13, 363–380.

Mitchel, J.T.D., George, M.W. 1972 A design concept for a fusion reactor blanket and a magnetic shield structure. UKAEA research group report, Culham Laboratory CLM-R121.

Molokov, S. 1993^a Fully developed liquid metal flow in multiple rectangular ducts in a strong uniform magnetic field. *KfK report*, KfK5075.

Molokov, S. 1993^b Fully developed liquid metal flow in multiple rectangular ducts in a strong uniform magnetic field. *Eur. J. Mech. B/Fluids*, 12, No.6,769–787

Molokov, S. 1994 Liquid metal flows in manifolds and expansions of insulating rectangular ducts in the plane perpendicular to a strong magnetic field. *KfK report*, KfK5272.

Molokov, S., Bühler, L. 1994 Liquid metal flow in a U-bend in a strong magnetic field. *J. Fluid Mech.* 267, 325–352.

Molokov, S. Shishko, A. 1993 Fully developed Magnetohydrodynamic flows in rectangular ducts with insulating walls. *KfK report*, KfK5247.

Moon, T.J., Hua, T.Q., Walker, J.S. 1991 Liquid-metal flow in a backward elbow in the plane of a strong magnetic field. *J. Fluid Mech.* **227**, 273–292.

Moon, T.J., Walker, J.S. 1990 Liquid-metal flow through a sharp elbow in the plane of a strong magnetic field. *J. Fluid Mech.* **223**, 397–418.

Morley, N.B., Tillack, M.S., Abdou, M.A. 1991 Development of an analytic core flow approximation for a square duct in an oblique magnetic field. *Report UCLA-FNT-46*, University of California Los Angeles.

O'Donnell, J.O., Papanikolaou, P.G., Reed, C.B. 1989 The thermophysical and transport properties of eutectic NaK near room temperature, *ANL report ANL/FPP/TM-237*.

Picologlou, B.F., Reed, C.B., Hua, T.Q., Barleon, L., Kreuzinger, H., Walker, J.S. 1989 Experimental investigations of MHD flow tailoring for first wall coolant channels of self-cooled blankets. *Fusion Technology* **15**, 1180–1185.

Reed, C.B., Picologlou, B.F. 1986 Techniques for measurement of velocity in liquid metal MHD-flows. 7th Top. Meeting on Fusion technology, Nevada.

Reed, C.B., Picologlou, B.F., Hua, T.Q., Walker, J.S. 1987 ALEX-results A comparison of measurements from a round and a rectangular duct with 3D-code predictions. 12th Symp. on Fus. Engng. IEEE, Monterey, Ca, Oct. 1987, 1267–1270.

Reimann, J., Molokov, S., Platnieks, I. Platacis, E. 1993 MHD flow in multi-channel U-bends: Screening experiments and theoretical analysis. *KfK report*, KfK5102.

Reimann, J. *et al.* 1994 MHD flow in a T-junction. To be published.

Shercliff, J.A. 1962 Magnetohydrodynamic Pipe flow. Part 2 *J. Fluid Mech.* **13**, 513–518.

Smith, P.L. et al. 1984 Blanket comparison and selection study (Final report), Argonne National Laboratory, report ANL/FPP-84.

Sterl, A. 1990 Numerical simulation of liquid-metal MHD flows in rectangular ducts. *J. Fluid Mech.* 216, 161-191.

Stieglitz, R. 1994 Magneto-hydrodynamische Strömungen in Ein- und Mehrkanalumlenkungen. *Dissertation, Universität Karlsruhe.*

Strandbridge, J.T., Curruthers, H.M., Keen, B.A., Shotter, H.A. Design of stainless steel blanket cell for a fusion reactor. UKAEA Research group report.

Sze, D.K., Mattas, R.F., Hull, A.B., Picologlou, B., Smith, D.L. 1992 MHD considerations for a self-cooled liquid lithium blanket. *Fusion Technology* 21, No.3, Part 2b, 2099-2106.

Talmage, G., Walker, J.S. 1987 Three-dimensional laminar MHD flows in ducts with thin metal walls and strong magnetic fields. Proc. of Beer Sheva conference on MHD and Turbulence 1987, Israel, 3-25.

Tillack, M.S. 1990 MHD flow in rectangular ducts. *Report UCLA-FNT-41, University of California Los Angeles.*

Walker, J.S. 1986 Liquid metal flow through a thin walled elbow in a plane perpendicular to a uniform magnetic field. *Int. J. Engng.Sci* 24, 1741-1754.

Walker, J.S. 1981 Magneto-hydrodynamic flows in rectangular ducts with thin conducting walls. *Journal de Méchanique* 20, No. 1, 79-112.

Walker, J.S., Ludford, G.S.S. 1974 MHD flow in insulating circular expansions with strong transverse magnetic fields. *Int. J. Engng.Sci* 12, 1045-1061.